The Aeronautical Journal (2023), **127**, pp. 1380–1434
doi:10.1017/aer.2023.12

REGULAR PAPER

Analysis of the traffic conflict situation for speed probability distributions

Zs. Öreg*, H.-S. Shin and A. Tsourdos

Centre for Autonomous and Cyber-Physical Systems, School of Aerospace, Transportation and Manufacturing, Cranfield University, Cranfield, UK
*Corresponding author. Email: zsombor.t.oreg@cranfield.ac.uk

Received: 14 August 2022; **Revised:** 22 January 2023; **Accepted:** 30 January 2023

Keywords: Autonomous systems; Unmanned traffic management; Analytical modelling; Air traffic conflict detection; Conflict detection analysis; Stochastic analysis

Abstract

The increasingly widespread application of drones and the emergence of urban air mobility leads to a challenging question in airspace modernisation: how to create a safe and scalable air traffic management system that can handle the expected density of operations. Increasing the number of vehicles in a given airspace volume and enabling routine operations are essential for these services to be economically viable. However, a higher density of operations increases risks, poses a great challenge for coordination and necessitates the development of a novel solution for traffic management. This paper contributes to the research towards such a strategy and the field of airspace management by calculating and analysing the conflict probability in an en-route, free-flight scenario for autonomous vehicles. Analytical methods are used to determine the directional dependence of conflict probabilities for exponential and normal prescribed speed probability distributions. The notions of geometric and speed conflict are introduced and distinguished throughout the calculations of the paper. The effect of truncating the set of available flight speeds is also investigated. The sensitivity of the calculated results to speed and heading perturbations is studied within the analytical framework and verified by numerical simulations. Results enable a fresh approach to conflict detection and resolution through distribution shaping and are intended to be used in an integrated, stochastic coordination framework.

Nomenclature

a	parameter of the exponential distribution for the ownship [−]
ACAS	airborne collision avoidance system
ADS-B	automatic dependent surveillance-broadcast
ATC	air traffic control
b	parameter of the exponential distribution for the intruder [−]
CA	collision avoidance
CNS	communication, navigation and surveillance
d	distance to be traversed between sensing range and conflict range[m]
DAA	detect and avoid
erfc	complementary error function
GC	geometric conflict
l	lower speed limit [Kn]
MDP	Markov decision process
NMAC	near mid-air collision
p	magnitude of normal distribution variables [−]
PAV	personal aerial vehicle
PDF	probability density function
Pr(x)	probability of x

© The Author(s), 2023. Published by Cambridge University Press on behalf of Royal Aeronautical Society. This is an Open Access article, distributed under the terms of the Creative Commons Attribution licence (https://creativecommons.org/licenses/by/4.0/), which permits unrestricted re-use, distribution, and reproduction provided the original article is properly cited.
https://doi.org/10.1017/aer.2023.12 Published online by Cambridge University Press

q	ratio of normal distribution variables ($q = x/y$), [−]
r	ratio of speeds [−]
r_C	conflict range [m]
r_S	sensing range [m]
sUAS	small unmanned aerial system
t_{th}	threshold time for speed conflict [s]
TCAS	traffic collision avoidance system
u	upper speed limit [Kn]
UAM	urban air mobility
UAS	unmanned aerial system
UAV	unmanned aerial vehicle
UTM	unmanned traffic management

Greek symbol

β	angle of projection of the conflict range on the sensing range [−]
γ	angle of the velocity triangle [−]
δ	angle at which the intruder becomes visible for the ownship - relative azimuth [−]
θ	relative heading angle of the intruder to the ownship [−]
λ	general exponential distribution parameter [−]
μ	parameter of the normal distribution for the ownship [−]
ν	parameter of the normal distribution for the intruder [−]
ρ	ratio of distribution parameters ($\rho = a/b$), [−]
σ	standard deviation of the normal distribution [−]
Ω	angle of the apparent path [−]

1.0 Introduction

1.1 Background and motivation

With the more frequent and widespread application of unmanned aerial vehicles (UAVs) [1], together with the advent of Personal Aerial Vehicles (PAVs) and Urban Air Mobility (UAM), the need for a novel traffic management framework emerges [2]. The current air traffic management methods cannot handle the rapid increase in the number of vehicles and the projected density of operations [3, 4]. This is due to the fact that the methods applied scale poorly because of their remote, centralised nature. Air traffic control was identified as one of the key constraints on urban air mobility (UAM) by Vascik and Hansman [3].

Thus a modernisation of airspace management is necessary. In order to make novel services related to UAVs and PAVs technically and commercially feasible it is desirable to create a mechanism for self-organising, in-flight strategic management which regulates airspace capacity. The traffic management system for UAM is expected to employ ideas from Unmanned Traffic Management to ensure scalability. Although, the UTM services would need to be tailored to the needs of UAM [5]. It has already been proven that conflicts involving a few aircraft can be solved easily and efficiently, satisfying assurances, even in a decentralised manner [6]. Therefore a potential goal of a traffic management system could be to create a framework that drives the probabilities of the formation of such conflict situations towards easily manageable scenarios even in complex, dense traffic [7].

1.2 Aim of the paper

Control of the density and complexity of traffic, and through that airspace capacity, is conjectured to be easiest by applying speed control from the set of possible ATC deconfliction methods (turns, vertical manoeuvres, speed changes) [6, 8]. Instead of controlling the speed of each individual aircraft, however, only the distribution of speed probabilities is controlled. A fundamental element of designing such a method, able to govern density and complexity, is understanding how conflicts occur in a speed

https://doi.org/10.1017/aer.2023.12 Published online by Cambridge University Press

distribution controlled airspace. The aim of this paper is to provide this self-contained element of the development process by providing a method to calculate the directional distribution of the conflict probability in a free-flight environment. In this environment, all aircraft are controlled to follow a prescribed speed probability distribution, taking into account that the range of available speeds is bounded. Results of the analysis are also applicable for main-flow systems [9].

1.3 Proposed solution

One way to ensure the necessary scalability and reliability of the system would be to design the coordination as a hierarchic system, similarly to frameworks proposed by Valavanis [10]. The framework proposed and analysed in this paper comprises three layers, all supervised by a human operator [3, 4]. At the base layer, the aim is to collect all nearby vehicles into ad-hoc formations in order to increase the airspace capacity. This can be achieved by applying flocking rules, similarly to the ones proposed by Huang, Tang and Lao [11]. For the middle layer, the objective is to coordinate these formations governing their behaviour based on the optimisation decisions of the top layer to maximise throughput while ensuring appropriate safety. The aim of the middle layer is not to provide deconfliction – tactical deconfliction within the formation and between formations is managed by the bottom layer using well-established techniques. The objective of the middle layer is to limit the probability of conflict resolution being necesary and present the ensemble to the top layer through a few, understandable parameters, namely the distribution parameters. Thus, the middle layer has to be able to govern global ensemble dynamics, ensuring all conflicts can be resolved by the bottom layer, while also taking care of throughput and remaining transparent at all times to the supervising control officers.

Although there is no one-to-one correspondence between the layers of the proposed model and conflict management system models [12] or concepts of operations for UAS [13, 14], the framework is in harmony with the recommendations and could possibly be integrated into the wider system-of-systems architecture. This paper focuses on the analysis of the middle layer of this framework. Previous results indicate that conflict probabilities and their distribution are related to the airspace performance metrics [15, 16]. Conflict rate (related to safety) and throughput (related to the average speed corrected for disruptions) describe system-level behaviour and enable overall airspace design.

1.4 Rationale

Within the middle layer, speed distribution control is achieved by applying a distributed stochastic task allocation method. This by design stochastic, distributed method was chosen for scalability and resilience, as it requires no central coordination and possesses a certain "self-repair" property [17]. However, the application of distributed stochastic task allocation requires analysis and necessitates the formulation of a methodology to determine how safely agents can operate.

In air traffic control practice the three resolution manoeuvres are horizontal (change in heading), vertical (change in flight level) and speed (change in flight speed) [6, 8]. For a given operation the starting point and the destination are considered given, loosely determining the heading angle. The instantaneous heading angle is necessary to be kept as a free variable to allow avoidance manoeuvres to deal with imminent conflicts. Altitude separation can be used as an effective way to increase airspace capacity. Since the focus of this paper is the middle layer and in-flight strategic management, the principal behaviour chosen to be regulated is the remaining degree of freedom, the control of the aircraft speed. Also, speed affects both throughput and the number of conflicts (safety), thus determining the optimal speed distribution is essential. Once this speed distribution is established, the middle layer can direct the formations towards that, using a distributed stochastic task allocation-based algorithm. This can be achieved using local information only, as presented by Jang, Shin and Tsourdos [18]. The middle layer function also contributes towards the self-optimisation characteristic of the framework described by Kopardekar [2].

https://doi.org/10.1017/aer.2023.12 Published online by Cambridge University Press

In order to control the number of decision variables, the type of distribution is prescribed. Ensemble dynamics can be controlled through the parameters of the distribution. Within the presented framework any arbitrary speed distribution can be analysed. Throughout this paper, exponential and normal distributions are investigated. Normal distribution can be regarded as analogous to ordinary traffic flow with disturbances. Analysis of en-route flight ground speeds based on traffic data resembles a normal distribution [19]. Exponential distribution would be beneficial for emergency situations (emergency services) since it permits much higher speeds than the average. Emergency vehicles can deterministically occupy these speed states, while other vehicles would automatically respond and adapt to maintain the prescribed distribution. The distributed stochastic task allocation method, however, would allow for any distribution to be prescribed as desired. To account for the fact that the set of available velocities is bounded in practice, the analysis is also performed for truncated distributions with lower and upper speed limits.

1.5 Assumptions and simplifications

Within the scope of this paper, the conflict situation is analysed for the ownship and a single intruder, to determine geometric and speed conflict probabilities and enhance collision detection. Results of previous research efforts are extended by generalising the conflict problem such that both the ownship and the intruder behave stochastically. Separation distances and speed ranges are defined to represent scenarios and characteristic dynamics of personal aerial vehicles (PAVs). Assuming independence of intruder behaviour, extension is straightforward for multiple intruders. Analysis of the effect of interdependence is subject to future work. Also, the analysis of the effect of human factors on operation is beyond the scope of this paper. Conflicts are analysed for level flying aircraft, in two dimensions, due to the complexity of the problem arising from the fact that speeds of participants are not given explicitly, only their distribution is known. Nevertheless, this simplified analysis in plane helps to create the calculation framework, gain insight and understand the underlying relations. Results about the shape of conflict probability distributions, the effect of truncation, sensitivity to perturbations and the comparison of different distributions are expected to be similar in 3D. Also, it is generally accepted [2, 4, 20, 21] that UAM PAVs would either fly in a narrow, dedicated altitude band, or the dedicated airspace will be segmented into layers to increase capacity. Extension with climbing and descending aircraft is left for future work. To preserve the generality of the results it is assumed that no conflict resolution technique is applied, thus the heading remains constant. Analysis of the effect of a particular resolution method, possibly designed based on current results, is left for future work.

1.6 Contribution of the paper

Results of this analysis can be integrated into the top-layer optimisation and middle-layer stochastic task allocation part of the framework. Directional probability distributions help decision making and optimisation. They also make the relationship between decision variables and ensemble dynamics better understood. The relationship between the overall conflict probability and the system-level metrics has been analysed previously [15, 16]. This paper provides a deeper insight by exploring the directionality of conflict probabilities. The results provide a benchmark and performance bounds for conflict resolution algorithms. In addition, providing bounds on conflict probabilities can lead to more effective conflict resolution algorithm design and enhanced risk management for the bottom layer. Studying the effect of distribution parameter selection and the ratio of parameters enables distribution shaping controlled by the selection of parameters. Moreover, results may help determine airspace capacity for specified safety criteria, and contribute towards orientation-based separation limits. Comparison of the conflict probability distributions resulting from prescribing exponential and normal speed distributions is important in relation to system-level safety. As results are calculated using analytical methods, accuracy and sensitivity to uncertainties can be determined in a straightforward manner. Distinguishing geometric and speed

https://doi.org/10.1017/aer.2023.12 Published online by Cambridge University Press

conflicts is an important step towards establishing the responsibilities and necessary dependability of the different levels of conflict detection algorithms, essential for a scalable management framework.

The paper is structured as follows. Research in aircraft conflict detection and conflict definitions are summarised in Section 2. Conflict probability calculations for exponential distribution are given in Section 3. For normal distribution, calculations are outlined in Section 4. Numerical verification methods and results are provided in Section 5. Results are analysed in Section 6, comparing the different distributions for geometric and speed conflicts.

Calculations throughout the paper were performed using Wolfram Mathematica. Verification simulations were implemented in Matlab.

2.0 Literature review

2.1 Definitions and context

Several, mostly different definitions for air traffic conflict and conflict detection methods can be found in the literature.

According to Kelly [22], a conflict can be defined either as a violation of the separation standard or the predicted violation of the separation. Separation is defined based on distance and protected zones of given shapes (oblate spheroid and cylinder). The notion of "conflict detection" and "conflict resolution" is distinguished. An alerting logic based on two protected zones is described, and the severity of the conflict is assessed based on the time to reach these ranges. Because of the different separation requirements, horizontal and vertical separation is treated separately. The proposed conflict detection algorithm is based on instantaneous state vectors and does not take into account the stochastic nature of the problem.

A review of conflict detection and resolution methods is presented by Kuchar and Yang [6], creating a taxonomy of the techniques applied. Conflict is defined as a loss of minimum separation for two or more aircraft. Detection and resolution techniques are characterised based on several characteristics: state propagation method (this paper presents a probabilistic approach), state dimensions (the paper introduces a model for the horizontal plane), detection capability, resolution capability, the type of resolution manoeuvre and the method to handle multiple conflicts (throughout the paper aircraft conflict probabilities are calculated in a pairwise manner). The paper also emphasises the importance of robustness and the need for a consistent benchmarking method.

A mathematical description of the TCAS (traffic collision avoidance system) logic is given by Tang, Zhu and Piera [23], and its capabilities are extended with horizontal resolution. TCAS is a last resort airborne system to prevent mid-air collisions by notifying the pilot of the threat (traffic advisory) and suggesting coordinated resolutions of the conflict situation (resolution advisory). The effect of surrounding traffic, induced risk, and resolution generated conflicts are also analysed using a graphical modelling and analysis software. With horizontal resolution, it is possible to reduce the domino effect. Taking into account induced conflicts is beneficial for airspace stability, however, no system-wide analysis is presented in the paper.

Formal mathematical definitions of conflict and collision can be found in the paper by Mitici and Blom [24], together with a comparative evaluation of collision probability estimation models. Several models are presented with their application areas and characteristics analysed in a unified mathematical framework. A survey of safety risk models and validation methods is also provided to reflect on their applicability. Presented methods may become useful in future aerospace design, especially for unmanned traffic management. None of the methods reviewed apply a method to govern global dynamics to keep conflict probability at an acceptable level and airspace complexity manageable.

2.2 Traffic collision avoidance systems

The ACAS (airborne collision avoidance system) was extended for unmanned systems (ACAS Xu) [25] and small unmanned systems (ACAS sXu) [26]. Collision detection is enabled by the surveillance and

https://doi.org/10.1017/aer.2023.12 Published online by Cambridge University Press

tracking module incorporating multiple surveillance inputs to determine the position of nearby aircraft, together with position uncertainty. The threat resolution module evaluates collision risk, taking into account surveillance and dynamic uncertainty and determines whether a resolution manoeuvre is necessary. Resolution manoeuvres may be horizontal, vertical or combined. Platform manoeuvrability is taken into account to ensure avoidance feasibility. The *sXu* variant has a different action space to reflect the capabilities of sUAS. The problem is modelled as a Markov decision process (MDP). The MDP problem is solved in real-time, coordinating with other aircraft if possible during run-time. Although multiple threats may be handled using utility decomposition and fusion, due to the MDP formulation and the "curse of dimensionality" (exponential growth of the state space with the number of agents) application in dense airspace is infeasible [27]. Therefore, managing airspace complexity on a higher level (middle layer of the framework proposed) is necessary and justifiable, with an underlying operation of an ACAS-like CA method, customised for UAM. It is worth noting, that the ACAS Xu operation is consistent with the model adopted in the framework investigated in the paper for lower-level collision avoidance.

In most of the algorithms, the future trajectory of the intruder aircraft is extrapolated based on a linear motion assumption [28, 29]. In the paper by Bilimoria [28], closed-form analytical solutions are presented based on geometric optimisation, producing trajectories with minimal deviation from nominal. Intruder trajectories are extrapolated based on current speed and heading. An instantaneous resolution manoeuvre is assumed, conflict can be resolved by changing heading only, speed only or both. It is assumed that both aircraft stay in the same horizontal plane, and no wind disturbance is taken into account. Multiple aircraft conflicts are resolved sequentially. Intruders are modelled as velocity obstacles by van den Berg *et al.* [29], it is assumed that agents do not change speed for a given lookahead time, and independently decide on their velocity for the next period without communication with other agents. In the paper, sufficient conditions for reciprocal *n*-body collision avoidance are derived. A key drawback of the algorithm presented is the assumption of perfect sensing, not taking into account any stochastic effect. Linear motion has been extended to curved trajectories by Zhong and Xuejun [30]. This is achieved by taking intent into account with predefined trajectory change points. To detect and resolve conflicts geometric optimisation can be used after projecting velocities to the piecewise linear trajectory. In all of the above-mentioned papers, a simple extrapolation is used for conflict detection, which may be efficient in a last resort avoidance manoeuvre, but permits no conclusions about performance, the effect on global dynamics and airspace capacity.

Conflict detection is simplified by Rebollo, Ollero and Maza [31] by discretising the space into cubic cells and sharing residence times, thus conflicts can be identified as time overlaps. Since the space is discretised, for collision avoidance graph-based methods can be used, namely the search tree algorithm and the tabu search algorithm. The key drawback of the methods is the need for the availability of information and scalability.

For fixed-wing aircraft, a collision avoidance algorithm is given based on manoeuvre coordination in the paper by Wan, Tang and Lao [32]. The set of possible manoeuvres is restricted to special manoeuvre styles, uncertainty is taken into account by a conical region calculated based on error radius. Conflicts are detected using the shared information on possible trajectories. Avoidance and manoeuvre selection is such that activation can be delayed as much as possible to minimise disruptions. For a given scenario the method proposed in the paper works appropriately, however, the effects of a manoeuvre on the wider airspace are not considered, thus, it may lead to a domino effect.

A self-organising collision avoidance method is presented by Huang, Tang and Lao [11] for approaching drone swarms. Self-organisation is achieved by applying a combination of Reynolds rules, extended with an anti-collision force, based on the pairwise closest point of approach, and linear extrapolation. Results show that rapid reorganisation creates a domino effect when using the traditional flocking rules only. This domino effect can be successfully overcome by self-coordination, demonstrating its effectiveness. The directionality of conflict probability, however, is not taken into account, even though it could lead to more efficient swarming.

https://doi.org/10.1017/aer.2023.12 Published online by Cambridge University Press

An automatic collision resolution algorithm is designed by Luongo, Di Vito and Corraro [33], based on an analytical solution for conflict detection. All aircraft applying the algorithm creates a self-organising system, assuming all aircraft share intent. Conflicts are resolved either by changing aircraft speed or by changing speed, flight path and track angle, respecting flight envelope. One of the requirements of the method was to solve all conflicts in a multi-aircraft scenario without creating new ones, thus induced conflicts are taken into account. Admittedly, not all conflict scenarios can be resolved. However, no method is given to identify such scenarios nor is any technique provided to avoid such scenarios or at least limit their probability.

Speed control is applied to minimise potential conflict by Constans, Fontaine and Fondacci [34]. The sliding horizon loop process is made up of two layers, the supervisory layer detects conflicts and calculates deconflicted arrival times using linear programming, while the localised control layer follows the set arrival times correcting for disturbances and respecting aircraft performance limits, applying predictive functional control. Conflicts are localised, they can only occur at route intersection points, therefore conflict detection is based on arrival times, and separation thus becomes time separation. Results show speed control is an effective and simple method to minimise conflict probability. The same space discretisation technique is described in the paper by Cecen and Cetek [35], focusing on en-route, level traffic. Speed control is identified as the long-term resolution method for conflicts. Airspace entry points are also considered variables of the optimisation problem, which is solved using a novel heuristic. The most important drawback of the above-described techniques is the need for a central entity for coordination.

2.3 Collision detection and risk

Analysis of collision detection methods is extended by taking into account the effect of navigation uncertainty and communication package losses in the paper by Mahjri *et al.* [36] UAVs flying in a straight line are assumed to exchange position and velocity information periodically. The effect of the setting of broadcast period and lookahead time on missed and false alarms is analysed analytically and using simulation. No conflict resolution method is applied so the performance of the detection algorithm could be analysed. The results presented are averaged over all relative headings, providing no insight into the underlying dynamics of the emergence of the conflict.

Collision risk as a result of UAS intruding terminal airspace is modelled by Wang, Tan and Low [37] to assess hazard and threat levels and prevent collisions with passenger aircraft. Based on an initial sighting of the UAS, its trajectory is propagated probabilistically to reflect on its "assumed intent". The position and state of the passenger aircraft are prescribed, and perfectly known to ATC. Conflict probability for a given scenario is calculated by 2D Monte-Carlo simulations resulting in a framework for risk management taking the maximum speed of the UAS model as an input. Alternatively, tracking data can be incorporated into decision making when available. The study highlights the importance of stochastic analysis in risk assessment. However, in this study, only one of the participating agents exhibits stochastic behaviour. Moreover, the evaluation is based solely on simulation results, which provides no help in understanding the underlying dynamics.

Another way to detect conflicts is to predict separation violations by calculating the reachable sets of intruders, taking intruder motion uncertainty into account. In the paper by Lin and Saripalli [38] a Dubins car model is used to represent obstacle aircraft kinematics, based on current information, assuming constant speed and limited maximal turning rate the reachable set can be calculated. The $x - y$ component and the z component of the set are calculated separately. To simplify the calculation, the reachable set is approximated by a polygon. The resolution path is generated using intermediate waypoint sampling. Although the method presented improves the success rate of collision avoidance, it does not take into account stochastic behaviour due to uncertain intent or disturbances, any relies on instantaneous information only, therefore does not reflect realistic collective dynamics.

A multi-aircraft conflict detection algorithm based on probabilistic reach sets is introduced by Yang *et al.* [39]. The nominal, piecewise linear trajectory of the aircraft is disturbed by a stochastic wind

https://doi.org/10.1017/aer.2023.12 Published online by Cambridge University Press

component, and possible realisations of the trajectory are formulated as a chance-constrained program, which is solved by the scenario approach to provide the ellipsoidal probabilistic reach sets. Conflicts are resolved as a second-order cone program. Utilising the algorithms described conflict detection can be accomplished for a given stochastic model, however, results are dependent on the given scenario and are therefore not universal.

A unified analytical framework for aircraft separation assurance and unmanned aircraft system sense-and-avoid is presented by Ramasamy, Sabatini and Gardi [40]. The paper presents mathematical models to calculate the overall uncertainty volume of the intruder aircraft, utilising unified range and bearing uncertainty descriptors, taking into account separation requirements. To determine the probability of near mid-air collisions, trajectory predictions and Monte Carlo approximations are used, based on cooperative and non-cooperative sensor selection and characteristics. Based on conflict identification the avoidance trajectory can be calculated as a result of an optimisation. For automated sensor selection, Adaptive Boolean Decision Logics are employed. Even though the paper represents a significant step towards certifiable separation assurance systems and determining UTM airspace capacity, a drawback of the methods described is that conflict probability can only be determined for a given scenario, using numerical models, therefore no general conclusions can be drawn, and the accuracy of the solutions remains uncertain.

For two common encounter geometries in a terminal manoeuvring area, a probabilistic conflict detection algorithm is formulated by Shi and Wu [41]. As a perturbation to the nominal trajectories, a three-dimensional Brownian motion is added and transformed to be standardised. Conflict probability is defined as the probability of the intruder entering the protection zone, which is the probability of a Brownian motion hitting a moving protection zone. Using the Bachelier-Levy theorem an analytical approximation is presented. Even though results can be used by air traffic control officers to assess the severity of a conflict for the analysed scenarios it is difficult to generalise the results of the paper.

Conflict detection for trajectory-based operations can also be found in the paper by Hao *et al.* [42]. Conflict probability is calculated taking into account random changes in pilot intent. The aim is to detect "whether two aircraft would violate the safe separation criteria during the look-ahead period based on the predicted aircraft trajectory". This is done by calculating the intersections of state-time prisms in a discretised space. The uneven occurrence probability distribution within the reachable domain is considered by the truncated Brownian bridge model. Multi-aircraft conflict probability is calculated assuming independence. Other than pilot intent, no source of uncertainty is taken into account.

2.4 Directional conflict probability

None of the papers listed describe any scenario when for both the ownship and the intruder behave according to given probabilities. Also, as it can be seen from the references cited, even though conflict probabilities are calculated by many, directional analysis for further insight is rarely given. An exception is a paper and a PhD thesis published by Hernández-Romero *et al.* [43, 44], which include directional analysis of the conflict probability according to the relative ground track angle of the two aircraft and the wind direction. A probabilistic approach to quantifying aircraft conflict intensity is presented, focusing on the propagation of wind forecast uncertainty using the probabilistic transformation method. The calculated conflict probability and intensity are used to improve optimal strategic deconfliction of aircraft trajectories under uncertainties derived from the ensemble weather forecast. This makes the research an important step towards minimising conflict probability taking into account weather uncertainty. Wind forecast uncertainties are relatively small compared to aircraft speeds used in the paper. Moreover, due to the small distance between the aircraft, the same wind is assumed to affect both aircraft, thus the uncertain wind vector added to the velocities is the same. In the current paper distribution parameters are not necessarily equal for both aircraft, providing a more general approach. While both papers highlight the importance of uncertainty analysis, the methodology presented here is better suited for high density airspace analysis and management, where the sources of uncertainty are more diverse.

https://doi.org/10.1017/aer.2023.12 Published online by Cambridge University Press

2.5 Aim of the paper

The aim of this paper is to provide analytical formulae for geometric and speed conflict probability evaluation. The analysis is performed without constraints of any specific scenario, in free flight. Calculation results using the formulae provided can serve as measures of effectiveness of prescribed distributions for the middle layer of the proposed framework. To assess the validity of the method no underlying conflict resolution technique is applied, similarly to Mahjri *et al.* [36]. Results of the analysis presented show how conflict probability is related to distribution parameters, which are to be used as decision variables in the top-level optimisation. Integrated analysis of the framework described in Section 1 is subject to future work.

3.0 Calculations for exponential distribution

In this section, the conflict situation is analysed with the speed of the ownship and the intruder both having exponential distributions. As already stated, an exponential speed distribution could be the best solution for enabling priority missions, e.g. emergency services. Calculation methods presented, however, are universal, and could be applied for any prescribed distribution, exponential distribution is merely an example.

Notations used are listed in NOMENCLATURE. Units used are generally accepted in the field of aerospace, albeit not standard, and thus not forming a metric system. Nevertheless, conversion constants are omitted from the formulae in the interest of clarity.

3.1 Definitions

To determine the probability of a conflict two ranges are defined around the ownship, the sensing (r_S) and the conflict range (r_C). It is assumed that the ownship becomes aware of the intruder once it enters the sensing range. A conflict may be defined as an event when the intruder enters a range (the conflict range) with a predefined radius around the ownship, which is referred to as *geometric conflict (GC)* throughout the paper. For an alternative definition for conflict it may be assumed that the ownship can avoid the intruder being too close (manoeuvring, possibly in cooperation with the intruding aircraft) given enough time, therefore a conflict is defined as the event when the intruder traverses from the sensing range to the conflict range faster than a threshold time (t_{th}). This event is referred to as a *speed conflict (SC)*. A conflict range value may be chosen as the NMAC (near mid-air collision) range or the well-clear range corresponding to the underlying DAA (detect and avoid) concept and method applied. As ACAS was extended to unmanned systems [25, 26], it is expected that UAM vehicles would have the same capability. NMAC and well-clear ranges in practice would be defined corresponding to this system, similarly to their derivation for small UAS [45, 46]. The above-described concept corresponds to a simplified model of the underlying collision avoidance performance requirements, defining the relevant volumes and time thresholds. This model is appropriate for the purposes of the investigation as the point is not to evaluate the capabilities of DAA systems but to determine conflict probabilities related to an encompassing system of the proposed framework. It is expected that performance requirements for UAM DAA systems would be standardised in the future, similarly to the requirements for unmanned aircraft [47].

The conflict geometry with the ranges and angle definitions can be seen in Fig. 1. The figure shows both the ownship and the intruder in the plane in which they are flying, in a coordinate system fixed to the ownship. Note that the figures are not to scale to help understanding.

The angle related to the projection of the conflict range on the sensing range is denoted by β and defined according to Equation (1). The angle at which the intruder becomes visible to the ownship is denoted by δ.

$$\sin(\beta) = \frac{r_C}{r_S} \tag{1}$$

https://doi.org/10.1017/aer.2023.12 Published online by Cambridge University Press

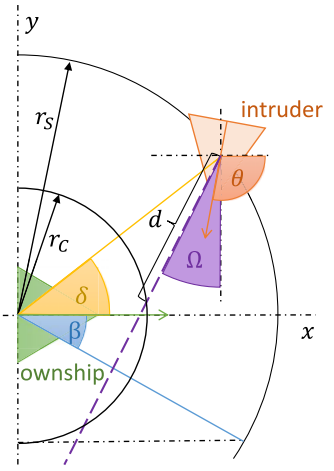

Figure 1. *The geometry of the scenario for which the conflict probabilities are calculated. The ownship and the intruder are flying in the same $x-y$ plane. Note that the figure is not to scale to help understanding.*

The formulae for conflict probabilities can be evaluated for arbitrary sensing and conflict ranges. For the plots in this paper the sensing and conflict ranges in Equations (2)–(4) were used, based on previous analysis on the flight and communication performance of UAM vehicles [15, 16].

$$r_C = 0.135\ [\text{nmi}] = 250\ [\text{m}] \tag{2}$$

$$r_S = 2.5\ [\text{nmi}] = 4630\ [\text{m}] \tag{3}$$

$$\beta = \arcsin\left(\frac{r_C}{r_S}\right) \approx 3.1^\circ \tag{4}$$

The speed of the ownship is denoted by v_{ownship}, and the speed of the intruder is v_{intruder}. Without loss of generality, the ownship is assumed to progress in the positive x-direction, and the angle between the intruder and ownship velocity is denoted by θ. The angle of the apparent path of the intruder is denoted by Ω.

For calculating the conflict probabilities for an intruder with perpendicular velocity it is convenient to express the ratio of speeds, which, considering the velocity triangle can be connected to the angle γ according to Equation (5).

$$r = \tan(\gamma) = \frac{v_{\text{ownship}}}{v_{\text{intruder}}} \tag{5}$$

Given the apparent position of the intruder and the angle of the apparent trajectory, the distance to be traversed to the conflict range can be calculated according to Equation (6).

$$d = \begin{cases} r_S \sin(\delta + \Omega) & \\ -r_S\sqrt{\sin^2(\delta+\Omega) - \cos^2\beta} & \text{if } \left(\delta - \beta \le \frac{\pi}{2} - \Omega \le \beta + \delta \text{ and } \Omega \ge -\frac{\pi}{2} \text{ and } \delta \ge \beta - \pi\right) \\ & \text{or } \left(-\beta \le \delta + \Omega + \frac{3\pi}{2} \le \beta \text{ and } \Omega \ge -\frac{\pi}{2} \text{ and } \delta \le \beta - \pi\right) \\ & \text{or } \left(-\beta \le \delta + \Omega + \frac{3\pi}{2} \le \beta \text{ and } \Omega < -\frac{\pi}{2} \text{ and } \delta \le \pi - \beta\right) \\ & \text{or } \left(\delta - \beta \le \frac{\pi}{2} - \Omega \le \beta + \delta \text{ and } \Omega < -\frac{\pi}{2} \text{ and } \delta \ge \pi - \beta\right) \\ \infty & \text{else} \end{cases} \tag{6}$$

https://doi.org/10.1017/aer.2023.12 Published online by Cambridge University Press

If the apparent trajectory is parallel to the movement of the ownship, Equation (6) can be simplified to Equation (7).

$$d_{\parallel} = \begin{cases} r_S \cos(\delta) - r_S\sqrt{\cos^2(\delta) - \cos^2(\beta)} & \text{if } -\beta \le \delta \le \beta \\ -r_S \cos(\delta) - r_S\sqrt{\cos^2(\delta) - \cos^2(\beta)} & \text{if } \delta \le -\pi + \beta \text{ or } \pi - \beta \le \delta \\ \infty & \text{if } -\pi + \beta \le \delta \le -\beta \\ & \text{or } \beta \le \delta \le \pi - \beta \end{cases} \tag{7}$$

Starting the investigations for the exponential distribution the probability distribution formulae are summarised. The probability density function and the cumulative distribution function of the exponential distribution are given by Equations (8) and (9), respectively.

$$f(x;\lambda) = \begin{cases} \lambda e^{-\lambda x} & \text{if } x \ge 0 \\ 0 & \text{if } x < 0 \end{cases} \tag{8}$$

$$F(X;\lambda) = \begin{cases} 1 - e^{-\lambda X} & \text{if } X \ge 0 \\ 0 & \text{if } X < 0 \end{cases} \tag{9}$$

Considering that the range of available speeds for an aircraft is limited (minimum speed due to stall and maximum speed due to performance and structural constraints) the effect of truncating the exponential distribution has to be taken into account as well. The probability density function and the cumulative distribution function of the truncated exponential distribution with lower limit l and upper limit u are given by Equations (10) and (11).

$$f'(x;\lambda,l,u) = \begin{cases} \dfrac{\lambda e^{-\lambda x}}{e^{-\lambda l} - e^{-\lambda u}} & \text{if } x \ge 0 \text{ and } l \le x \le u \\ 0 & \text{else} \end{cases} \tag{10}$$

$$F'(X;\lambda,l,u) = \begin{cases} \dfrac{e^{\lambda u}\left(-1 + e^{\lambda(l-X)}\right)}{e^{-\lambda l} - e^{-\lambda u}} & \text{if } X \ge 0 \text{ and } l \le X \le u \\ 1 & \text{if } X > u \\ 0 & \text{else} \end{cases} \tag{11}$$

For the ownship and the intruder, the parameters of the exponential distribution are denoted by a and b respectively, thus the cumulative distribution functions of the speeds become as given by Equations (12) and (13) for the non-truncated distributions.

$$\Pr\left(v_{\text{ownship}} \le X\right) = 1 - e^{-aX} \tag{12}$$

$$\Pr(v_{\text{intruder}} \le Y) = 1 - e^{-bY} \tag{13}$$

The formulae derived for conflict probabilities can be evaluated for arbitrary distribution parameters and speed limits. Based on previous analysis on the flight and communication performance of UAM vehicles [15, 16], for the plots in this paper the parameter ranges and speed limits in Equations (14)–(16) were used for exponential distribution.

$$a \in [0.0025, 0.2]\,, b \in [0.0025, 0.2] \tag{14}$$

$$l = 15\ [\text{Kn}] \tag{15}$$

$$u = 180\ [\text{Kn}] \tag{16}$$

https://doi.org/10.1017/aer.2023.12 Published online by Cambridge University Press

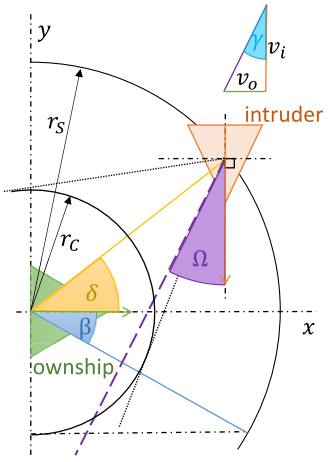

Figure 2. *The geometry of the conflict scenario for perpendicular velocities. The ownship and the intruder are flying in the same $x-y$ plane. Note that the figure is not to scale to help understanding.*

The mean speeds for the chosen parameter range and speed limits for the truncated exponential distribution are shown in Fig. 3. Generally, higher values of the rate parameter (a or b) indicate lower mean speeds.

For the conflict probability calculations, it is necessary to calculate the sum, the difference and the ratio of exponentially distributed random variables. All related formulae can be found in Appendix A.1.

3.2 Probability of entering the conflict range for perpendicular velocities

Even though an intruder may appear from any direction on the sensing range circle as a first approximation the principal directions are analysed. Derivation for these principal directions is useful in itself for airspace structures with constrained principal directions [21]. Moreover, based on these primary formulae arbitrary directions or their superposition may be analysed.

The conflict geometry for this scenario is shown in Fig. 2.

Assuming the velocity of the intruder is *perpendicular* to the velocity of the ownship, no conflict occurs if Equation (17) holds.

$$\begin{cases} \gamma < \dfrac{\pi}{2} - (\delta + \beta) & \text{if } -\beta \le \delta \le \dfrac{\pi}{2} - \beta \\ \gamma > \dfrac{\pi}{2} - (\delta - \beta) & \text{if } \beta \le \delta \le \dfrac{\pi}{2} + \beta \end{cases} \tag{17}$$

The conditions can be transformed according to Equations (18) and (19).

$$\tan(\gamma) < \tan\left(\frac{\pi}{2} - (\delta + \beta)\right) = \cot(\delta + \beta) \tag{18}$$

$$\tan(\gamma) > \tan\left(\frac{\pi}{2} - (\delta - \beta)\right) = \cot(\delta - \beta) \tag{19}$$

Therefore the probabilities that no conflict occurs become as given by Equations (20) and (21) for ranges defined in Equation (17), using the formula derived in Equation (58)

$$\Pr(r \le \cot(\delta + \beta)) = \frac{a\cot(\delta + \beta)}{a\cot(\delta + \beta) + b} \tag{20}$$

https://doi.org/10.1017/aer.2023.12 Published online by Cambridge University Press

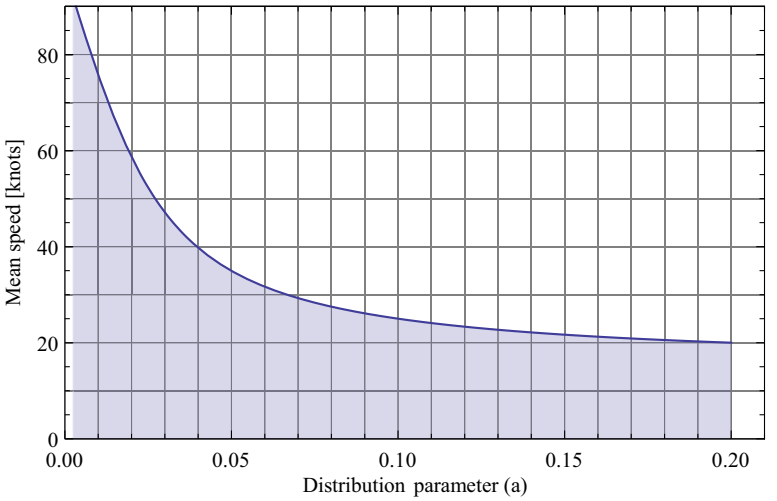

Figure 3. *Mean speed in Kn as a function of the exponential distribution parameter (a for the ownship and b for the intruder).*

$$\Pr(r \geq \cot(\delta - \beta)) = \frac{b}{a\cot(\delta - \beta) + b} \tag{21}$$

Thus, for the ranges of δ where conflict is possible, defining the parameter ratio as $\rho = a/b$, the probabilities become the following.

Case 1: $-\beta \leq \delta \leq \beta$

$$\Pr_{\text{perp}}(\text{GC}) = \frac{b}{a\cot(\beta + \delta) + b} = \frac{1}{\rho\cot(\beta + \delta) + 1} \tag{22}$$

Case 2: $\beta \leq \delta \leq \frac{\pi}{2} - \beta$

$$\Pr_{\text{perp}}(\text{GC}) = \frac{b}{a\cot(\beta + \delta) + b} + \frac{b}{a\cot(\beta - \delta) - b} = \frac{1}{\rho\cot(\beta + \delta) + 1} + \frac{1}{\rho\cot(\beta - \delta) - 1} \tag{23}$$

Case 3: $\frac{\pi}{2} - \beta \leq \delta \leq \frac{\pi}{2} + \beta$

$$\Pr_{\text{perp}}(\text{GC}) = 1 - \frac{b}{b - a\cot(\beta - \delta)} = 1 - \frac{1}{1 - \rho\cot(\beta - \delta)} \tag{24}$$

Conflict probability formulas can be evaluated for arbitrary ratio of distribution parameters (ρ) yielding conflict probability distribution for the full circle (Figs. 4 and 5). It can be seen that for equal distribution parameters ($\rho = 1$) the highest probability of a conflict occurs at head-on or perpendicular encounters. This corresponds to predicted behaviour, because with equal parameters the expected value of speed is the same, thus for an intruder arriving from a perpendicular direction the distribution is symmetric to $\pi/4$ with peaks at β and $\pi/2 - \beta$. By modifying the ratio of distribution parameters the distribution of conflict probability can be adjusted. For $\rho = 80$ the conflict probability for the $-\beta$ to $\pi/2 - \beta$ region reduces almost completely, but increases significantly in the $\pi/2 - \beta$ to $\pi/2 + \beta$ range. Opposite, but symmetric behaviour can be seen for $\rho = 1/80$.

If the set of available speeds is bounded, and the velocity magnitudes assume a truncated distribution, the conflict probabilities can be calculated according to Equations (61), (62) and (63) (Appendix A.2), using the results in Equation (60).

https://doi.org/10.1017/aer.2023.12 Published online by Cambridge University Press

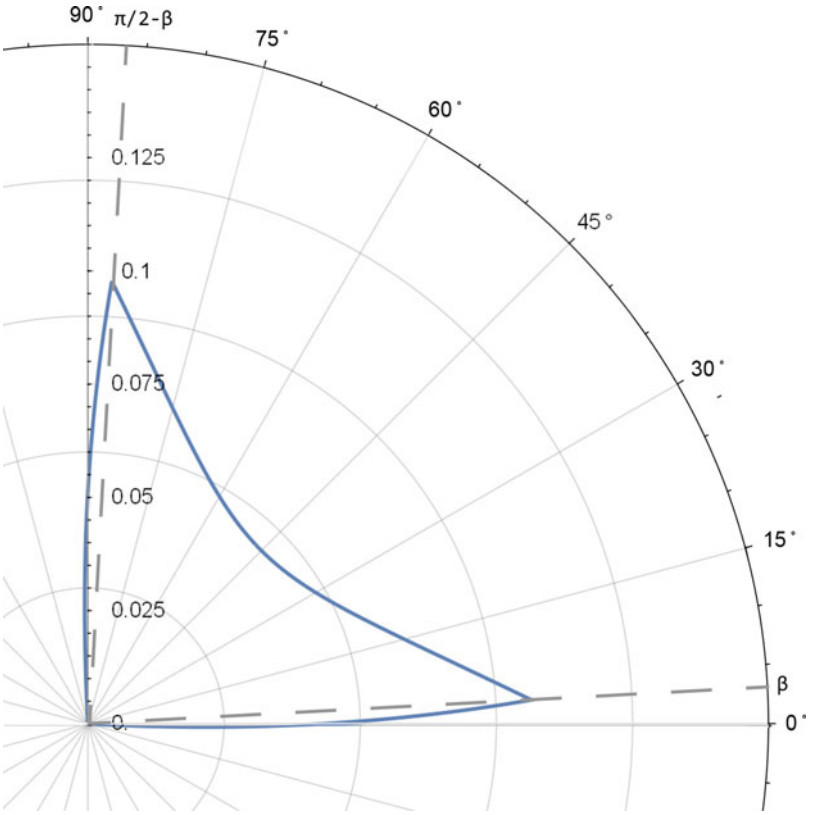

Figure 4. *Polar plot showing the probability of geometric intrusion with perpendicular intruder velocity for exponential distribution with* $\rho = 1$ *(*$a = 0.0025$ *and* $b = 0.0025$*,* $\theta = \frac{\pi}{2}$*). The radius coordinate represents conflict probability magnitude, while the angle coordinate shows relative azimuth.*

As it can be seen in Figs. 6 and 7 the probability distribution changes significantly if the bounds considerably affect the range of available speeds ($l = 15,\ u = 180$). Relaxing the bounds ($l = 0,\ u = \infty$) provides the unbounded results. If the distribution is truncated, the point of maximum conflict probability shifts to $\pi/4$ for equal parameters. Not only the angle but also the magnitude of the peak probability changes. For $\rho = 80$ the peak probability decreases considerably and tilts back towards $\pi/4$.

Since conflict probability formulae are given analytically, the sensitivity of results to parameter changes can be evaluated by calculating the partial derivatives with respect to the parameters. The analysis method is presented for geometric conflict probability with exponential distributions (given by Equations (22)–(24)), and it can be applied for all subsequent scenarios. The partial derivative with respect to the distribution parameter ratio (ρ) can be calculated as in Equation (25).

$$\frac{\partial \underset{\text{perp}}{\Pr(\text{GC})}}{\partial \rho} = \begin{cases} -\dfrac{\cot(\beta+\delta)}{(\rho\cot(\beta+\delta)+1)^2} & \text{if } \beta+\delta \geq 0 \text{ and } \beta-\delta \geq 0 \\ -\dfrac{\cot(\beta-\delta)}{(\rho\cot(\beta-\delta)-1)^2} - \dfrac{\cot(\beta+\delta)}{(\rho\cot(\beta+\delta)+1)^2} & \text{if } \beta-\delta \leq 0 \text{ and } \beta+\delta \leq \dfrac{\pi}{2} \\ \dfrac{\cot(\beta-\delta)}{\rho\cot(\beta-\delta)-1} - \dfrac{\rho\cot^2(\beta-\delta)}{(\rho\cot(\beta-\delta)-1)^2} & \text{if } \beta+\delta \geq \dfrac{\pi}{2} \text{ and } \beta-\delta \geq -\dfrac{\pi}{2} \end{cases} \tag{25}$$

Sensitivity as a function of heading difference can be seen in Fig. 8. Overall, the magnitude of change with parameter variation is very low. Although there are no explicit metrics for parameter sensitivity,

https://doi.org/10.1017/aer.2023.12 Published online by Cambridge University Press

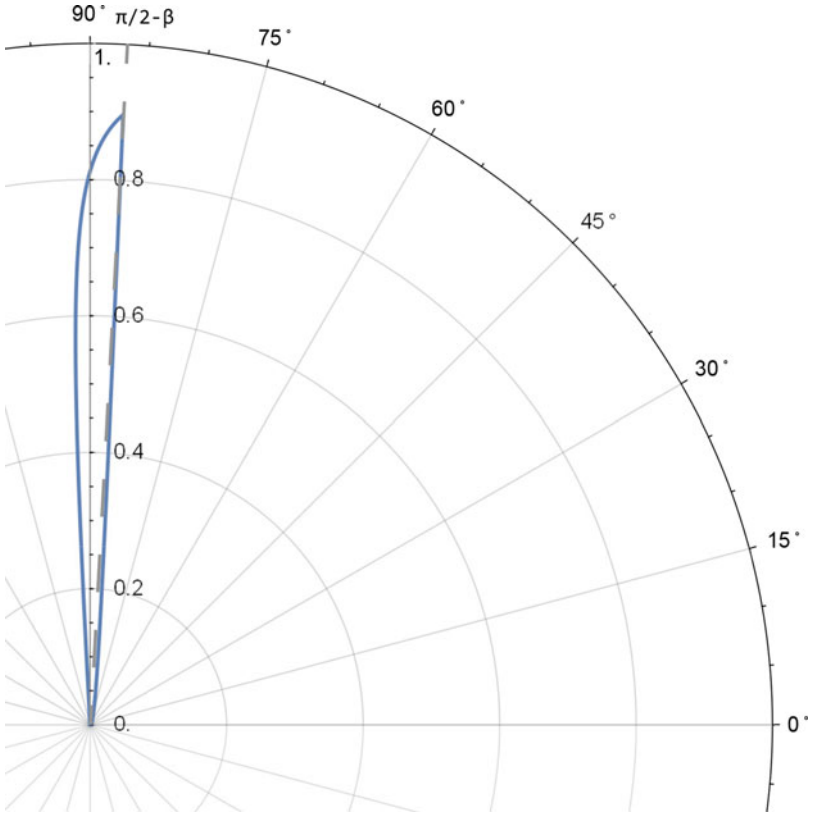

Figure 5. *Polar plot showing the probability of geometric intrusion with perpendicular intruder velocity for exponential distribution with* $\rho = 80$ *(*$a = 0.2$ *and* $b = 0.0025$*,* $\theta = \frac{\pi}{2}$*). The radius coordinate represents conflict probability magnitude, while the angle coordinate shows relative azimuth.*

it is still meaningful to calculate the sensitivities to parameters as they indicate how the result changes with input perturbations. Maximum locations of conflict probability and its sensitivity curve coincide. This is expected, as $\rho = 1$ represents a limiting case. For $\rho = 80$, shown in Fig. 9, sensitivity is even lower, the peak location is at a low conflict probability angle, $\delta = \frac{\pi}{2} + \beta$. This is because conflict at this heading difference is almost only possible at an extreme ratio, even a slight perturbation of the parameter results in a significant change in probability.

For truncated distributions, since conflict probability is not only a function of the parameter ratio, sensitivities were determined for the distribution parameters separately as shown in Figs. 10 and 11. For low parameter values, the change with parameter perturbation is significant due to the characteristics of the probability density function of the exponential distribution. As the parameter values increase the sensitivity decreases. Nevertheless, conflict probability for truncated distributions is still predominantly determined by parameter ratio, insensitivity to perturbations will be shown in Section 5.

3.3 Probability of entering the conflict range for parallel velocities

As another principal direction parallel velocities can be analysed. The conflict geometry for parallel velocities is shown in Fig. 12.

Considering geometric conflicts only, if the velocities of the ownship and the intruder are not only parallel, but point in the opposite direction a conflict surely occurs ($\Pr(\mathrm{GC}) = 1$) if the intruder is in the

https://doi.org/10.1017/aer.2023.12 Published online by Cambridge University Press

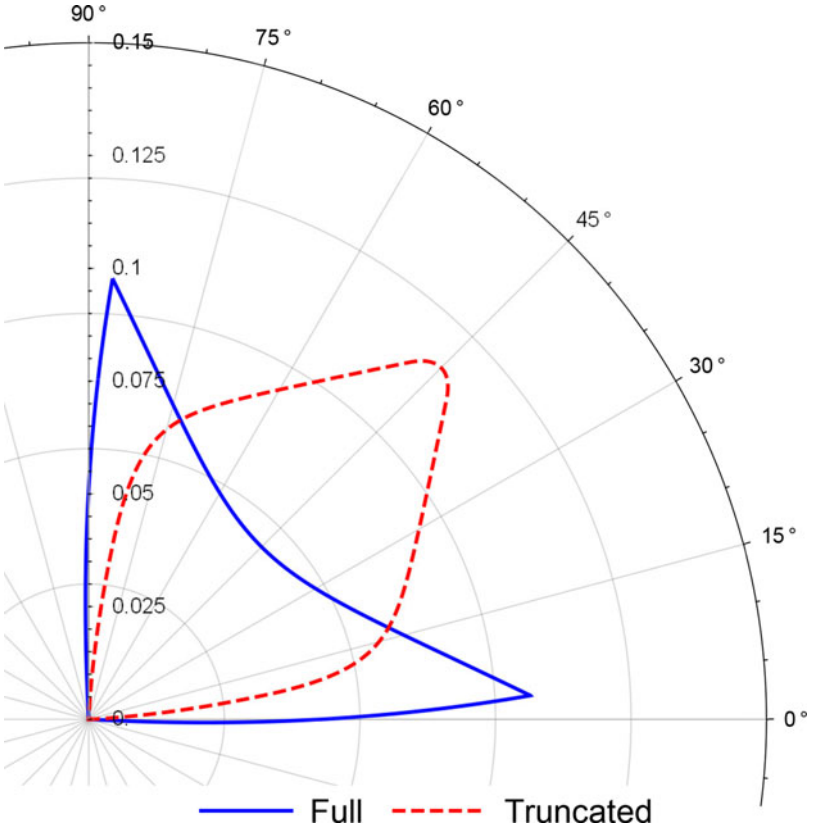

Figure 6. *Polar plot showing the probability of geometric intrusion with perpendicular intruder velocity for truncated exponential distribution with* $\rho = 1$ *(*$a = 0.0025$ *and* $b = 0.0025$*,* $\theta = \frac{\pi}{2}$*,* $l = 15$*,* $u = 180$*). The radius coordinate represents conflict probability magnitude, while the angle coordinate shows relative azimuth.*

range of the projection of the conflict range on the sensing range (Equation (26)).

$$\Pr_{\text{parallel}}(\text{GC}) = \begin{cases} 1 & \text{if } -\beta < \delta < \beta \\ 0 & \text{if } \delta \leq -\beta \text{ or } \beta \leq \delta \end{cases} \tag{26}$$

If the velocities point in the same direction, a geometric conflict occurs only if the intruder is in the angle range determined by the projection of the conflict range, and its speed is greater than the speed of the ownship if the intruder is behind (the difference of speeds is positive ($y - x > 0$), Equation (27), or the intruder speed is less than the ownship speed, and the intruder is ahead. Calculations are based on Equation (54)).

$$\Pr_{\text{parallel}}(\text{GC}) = \begin{cases} \dfrac{a}{a+b} & \text{if } \delta < -\pi + \beta \text{ or } \pi - \beta < \delta \\ \dfrac{b}{a+b} & \text{if } -\beta < \delta < \beta \\ 0 & \text{if } -\pi + \beta \leq \delta \leq -\beta \\ & \text{or } \beta \leq \delta \leq \pi - \beta \end{cases} \tag{27}$$

https://doi.org/10.1017/aer.2023.12 Published online by Cambridge University Press

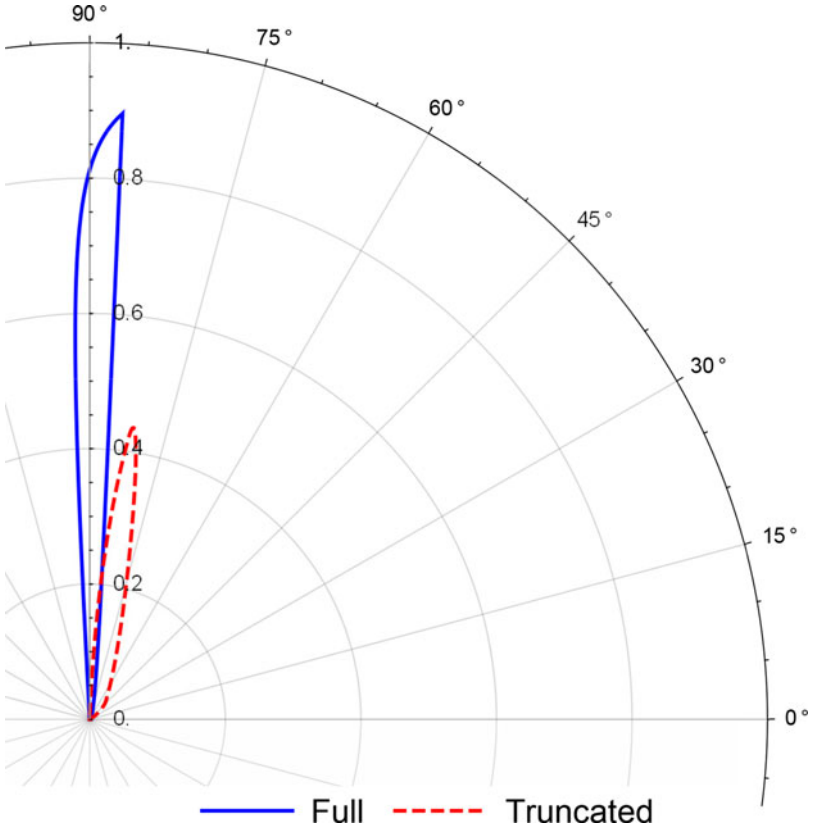

Figure 7. *Polar plot showing the probability of geometric intrusion with perpendicular intruder velocity for truncated exponential distribution with* $\rho = 80$ *(*$a = 0.2$ *and* $b = 0.0025$*,* $\theta = \frac{\pi}{2}$*,* $l = 15$*,* $u = 180$*). The radius coordinate represents conflict probability magnitude, while the angle coordinate shows relative azimuth.*

If the distributions are truncated, the probability of a positive difference becomes different as given by Equation (28) (based on Equation (56)).

$$\Pr_{\text{parallel}}(\text{GC}') = \begin{cases} \dfrac{e^{al}\left(ae^{bl} - (a+b)e^{bu}\right) + be^{u(a+b)}}{(a+b)\left(e^{al} - e^{au}\right)\left(e^{bl} - e^{bu}\right)} & \text{if } \delta < -\pi + \beta \text{ or } \pi - \beta < \delta \\ \dfrac{be^{bl}\left(e^{al} - e^{au}\right) + a\left(e^{u(a+b)} - e^{au+bl}\right)}{(a+b)\left(e^{al} - e^{au}\right)\left(e^{bl} - e^{bu}\right)} & \text{if } -\beta < \delta < \beta \\ 0 & \text{if } -\pi + \beta \le \delta \le -\beta \\ & \text{or } \beta \le \delta \le \pi - \beta \end{cases} \tag{28}$$

Having taken into account all possibilities with parallel and perpendicular intruder velocities, assuming that they have a uniform probability, the composite probability distributions weighted by arc lengths can be determined, as shown in Figs. 13 and 14. Even though the probability of head-on and rear-end collisions is much higher than that of perpendicular collisions, when weighted with the corresponding

https://doi.org/10.1017/aer.2023.12 Published online by Cambridge University Press

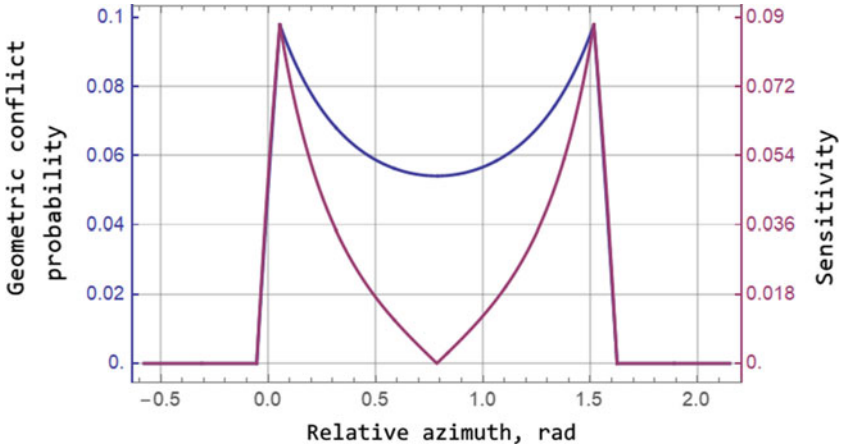

Figure 8. *Sensitivity of geometric intrusion probability to changes in parameter ratio of exponential distribution with perpendicular intruder velocity ($\rho = 1$, $a = 0.0025$ and $b = 0.0025$, $\theta = \frac{\pi}{2}$). As a function of relative azimuth angle, geometric intrusion probability is shown on the left axis, and sensitivity is shown on the right axis.*

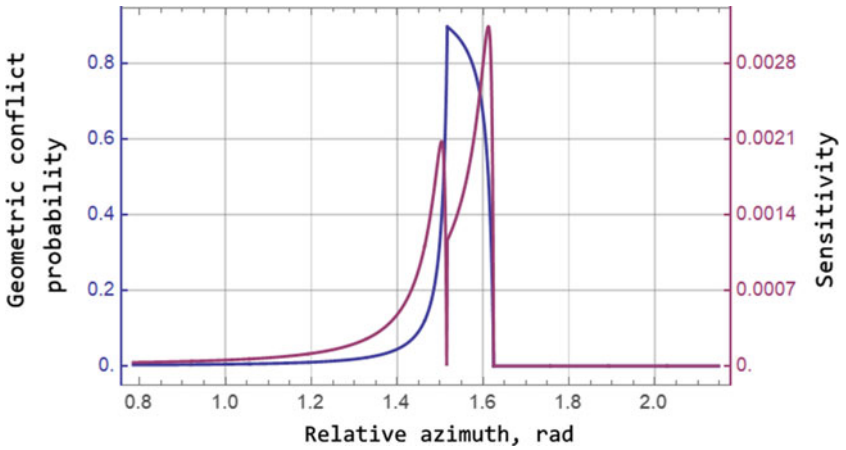

Figure 9. *Sensitivity of geometric intrusion probability to changes in parameter ratio of exponential distribution with perpendicular intruder velocity ($\rho = 80$, $a = 0.2$ and $b = 0.0025$, $\theta = \frac{\pi}{2}$). As a function of relative azimuth angle, geometric intrusion probability is shown on the left axis, and sensitivity is shown on the right axis.*

arc length it decreases below the perpendicular probability, especially in the truncated case, where the contribution of the perpendicular probability is not as significant in these directions.

3.4 Probability of entering the conflict range for velocities with arbitrary direction

To generalise the results obtained in the previous sections the geometric conflict probability is analysed for arbitrary intruder velocity angles (θ) as well. The angle of the apparent path (Ω) can be calculated based on the relative equations of motion, according to Equation (29).

https://doi.org/10.1017/aer.2023.12 Published online by Cambridge University Press

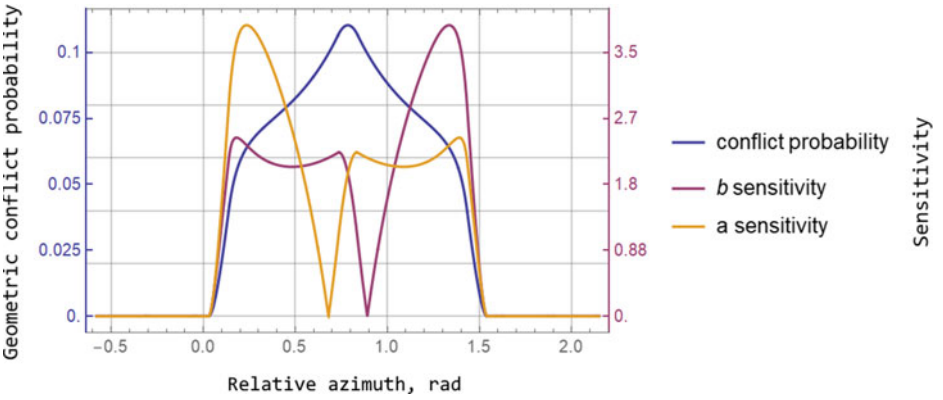

Figure 10. *Sensitivity of geometric intrusion probability to changes in parameters of truncated exponential distributions with perpendicular intruder velocity ($\rho = 1$, $a = 0.0025$ and $b = 0.0025$, $\theta = \frac{\pi}{2}$, $l = 15$, $u = 180$). As a function of relative azimuth angle, geometric intrusion probability is shown on the left axis, and sensitivity is shown on the right axis.*

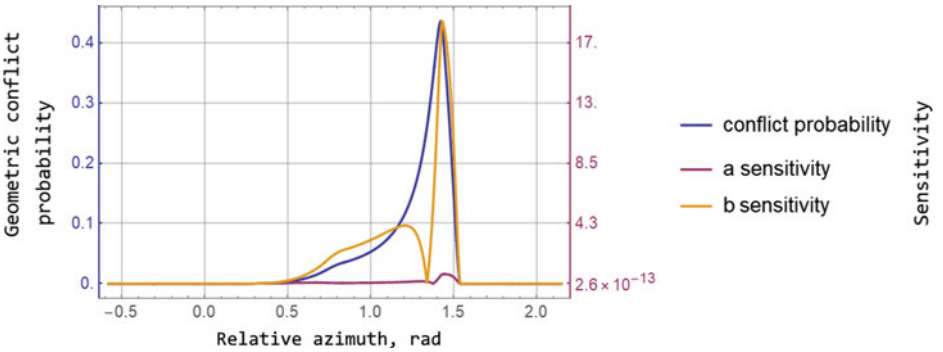

Figure 11. *Sensitivity of geometric intrusion probability to changes in parameters of truncated exponential distributions with perpendicular intruder velocity ($\rho = 80$, $a = 0.2$ and $b = 0.0025$, $\theta = \frac{\pi}{2}$, $l = 15$, $u = 180$). As a function of relative azimuth angle, geometric intrusion probability is shown on the left axis, and sensitivity is shown on the right axis.*

$$\Omega = \begin{cases} \arctan\left(\dfrac{\tan\gamma}{\sin\theta} + \cot\theta\right) & \text{if } 0 < \theta < \pi \\ \pi + \arctan\left(\dfrac{\tan\gamma}{\sin\theta} + \cot\theta\right) & \text{if } -\pi < \theta < 0 \\ \dfrac{\pi}{2} & \text{if } \theta = 0 \\ \dfrac{\pi}{2} & \text{if } \theta = \pi \text{ and } v_A \geq v_B \\ -\dfrac{\pi}{2} & \text{if } \theta = \pi \text{ and } v_A < v_B \end{cases} \tag{29}$$

In Equation (29) the angle θ is measured from the negative x-axis, in the clockwise direction and Ω is measured from the negative y-axis in the anticlockwise direction. Since it is easier to calculate the

https://doi.org/10.1017/aer.2023.12 Published online by Cambridge University Press

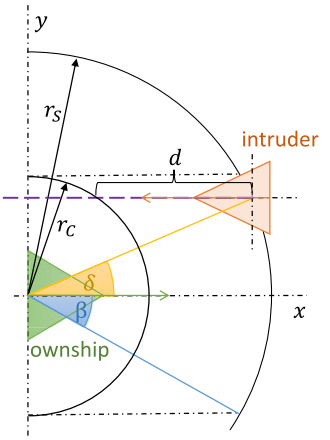

Figure 12. *The geometry of the conflict scenario for parallel velocities. The ownship and the intruder are flying in the same $x-y$ plane. Note that the figure is not to scale to help understanding.*

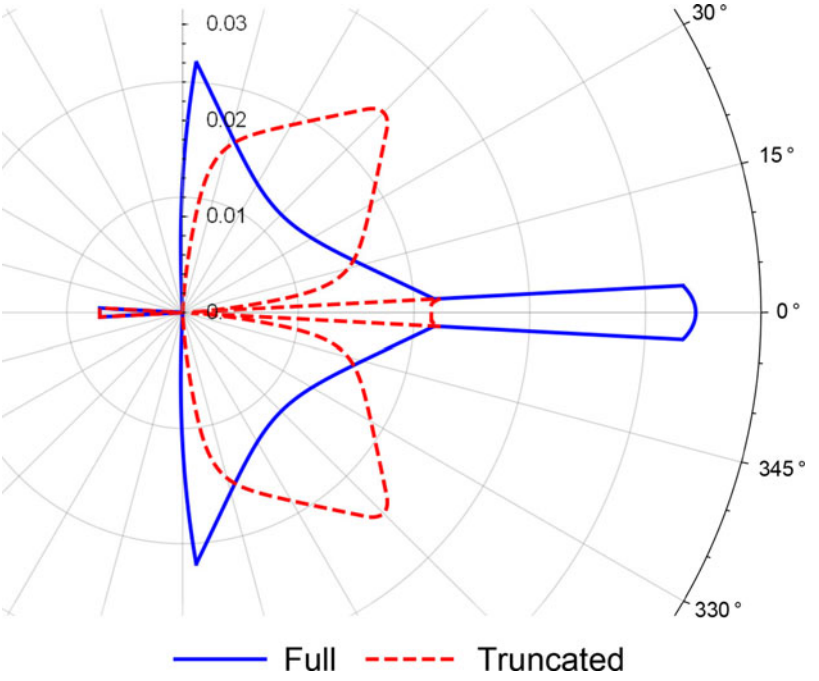

Figure 13. *Polar plot showing the probability of geometric intrusion with equally likely perpendicular and parallel intruder velocities for full and truncated exponential distribution with $\rho = 1$ ($a = 0.0025$ and $b = 0.0025$, $\theta = \left\{\frac{\pi}{2}, 0, -\frac{\pi}{2}, \pi\right\}$, $l = 15$, $u = 180$). The radius coordinate represents conflict probability magnitude, while the angle coordinate shows relative azimuth.*

probability distribution of the tangent of the apparent path angle (Equation (30), based on Equation (58)), the conflict probability limits for $0 < \theta < \pi$ were transformed according to Equation (31) and (32).

$$\Pr(\tan\Omega \le Z) = \begin{cases} \dfrac{a\sin\theta(Z-\cot\theta)}{a\sin\theta(Z-\cot\theta)+b} & \text{if } \cot\theta \le Z \\ 0 & \text{if } \cot\theta > Z \end{cases} \tag{30}$$

https://doi.org/10.1017/aer.2023.12 Published online by Cambridge University Press

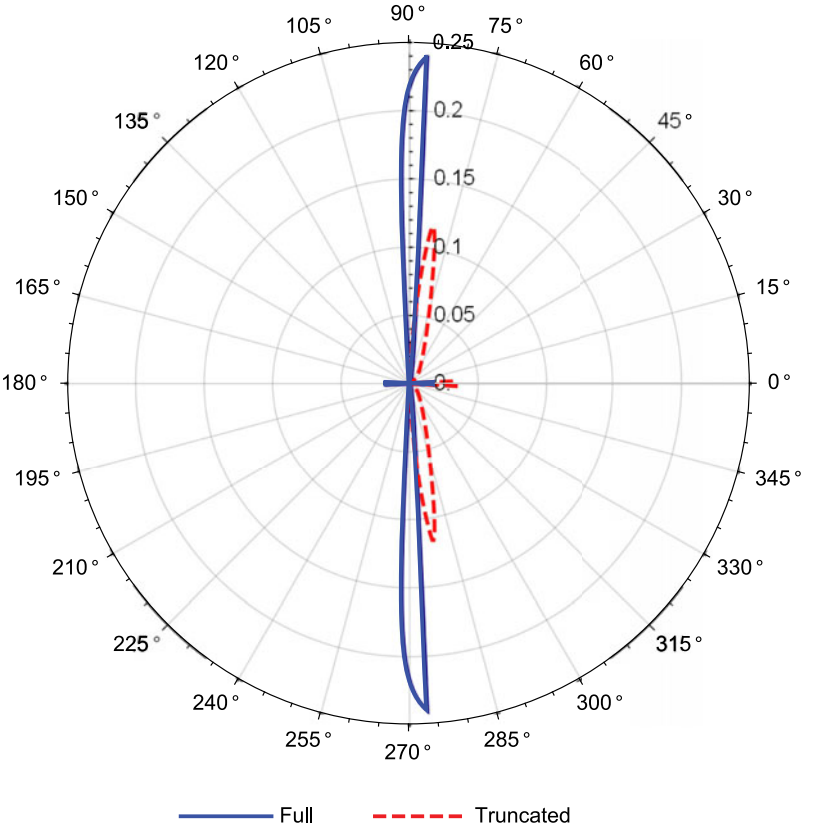

Figure 14. *Polar plot showing the probability of geometric intrusion with equally likely perpendicular and parallel intruder velocities for full and truncated exponential distribution with* $\rho = 80$ *(*$a = 0.2$ *and* $b = 0.0025$*,* $\theta = \left\{\frac{\pi}{2}, 0, -\frac{\pi}{2}, \pi\right\}$*,* $l = 15$*,* $u = 180$*). The radius coordinate represents conflict probability magnitude, while the angle coordinate shows relative azimuth.*

$$\begin{cases} \dfrac{\pi}{2} - (\delta + \beta) \le \Omega \le \dfrac{\pi}{2} & \text{if } -\beta \le \delta \le \beta \\ \dfrac{\pi}{2} - (\delta + \beta) \le \Omega \le \dfrac{\pi}{2} - (\delta - \beta) & \text{if } \beta < \delta < \pi - \beta \\ -\dfrac{\pi}{2} \le \Omega \le \dfrac{\pi}{2} - (\delta - \beta) & \text{if } -\pi \le \delta \le -\pi + \beta \text{ or } \pi - \beta \le \delta \le \pi \end{cases} \tag{31}$$

$$\begin{cases} \cot(\delta + \beta) \le \tan\Omega & \text{if } -\beta \le \delta \le \beta \\ \cot(\delta + \beta) \le \tan\Omega \le \cot(\delta - \beta) & \text{if } \beta < \delta < \pi - \beta \\ \tan\Omega \le \cot(\delta - \beta) & \text{if } -\pi \le \delta \le -\pi + \beta \text{ or } \pi - \beta \le \delta \le \pi \end{cases} \tag{32}$$

Calculations of conflict probabilities can be found in Appendix A.3.

Figures 15, 16, 17 and 18 show the conflict probabilities for $\theta = \frac{\pi}{4}$ and $\theta = \frac{3\pi}{4}$ with full and truncated distributions. It can be seen, that having an arbitrary angle for intrusion corresponds to an angular scaling with the origin being the centre. For $\rho = 80$ and $\theta = \pi/4$ the angle for maximum conflict probability shifts from $\pi/2$ to $\pi/4$. For truncated distributions, the same reduction and shifting behaviour is visible as in Fig. 7 for $\rho = 80$. For $\rho = 1$, the distribution is modified similarly as it can be seen in Fig. 6.

https://doi.org/10.1017/aer.2023.12 Published online by Cambridge University Press

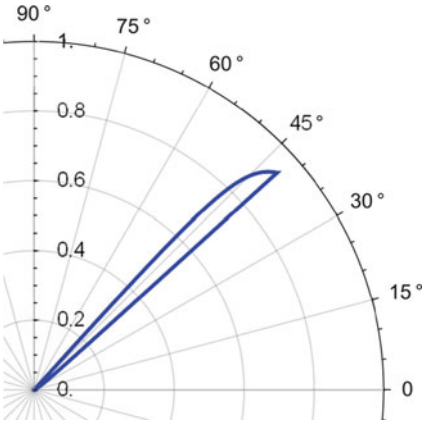

Figure 15. *Polar plot showing the probability of geometric intrusion for $\theta = \frac{\pi}{4}$, exponential distribution with $\rho = 80$ ($a = 0.2$ and $b = 0.0025$, $\theta = \frac{\pi}{4}$). The radius coordinate represents conflict probability magnitude, while the angle coordinate shows relative azimuth.*

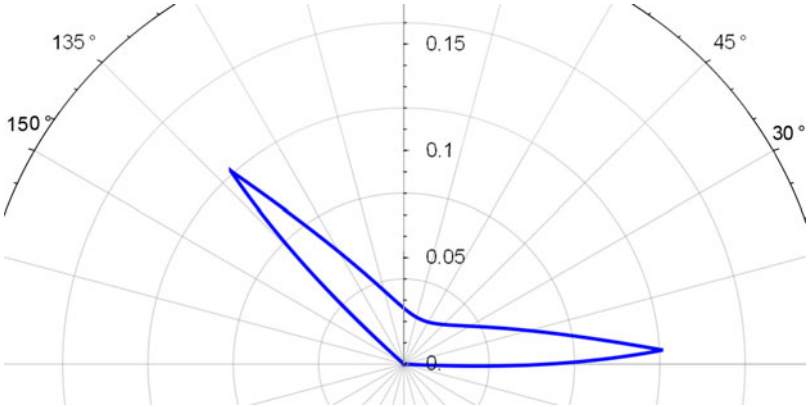

Figure 16. *Polar plot showing the probability of geometric intrusion for $\theta = \frac{3\pi}{4}$, exponential distribution with $\rho = 1$ ($a = 0.0025$ and $b = 0.0025$, $\theta = \frac{3\pi}{4}$). The radius coordinate represents conflict probability magnitude, while the angle coordinate shows relative azimuth.*

3.5 Probability of entering the conflict range for velocities with uniform distribution of intrusion angle

To evaluate the probability of conflicts in a realistic free flight traffic scenario, assuming a uniform distribution for intrusion velocity angles the conflict probabilities were averaged for all intrusion angles as shown in Fig. 19. If the distribution of intrusion relative headings is not uniform, but known, the same method may be applied as a weighted average, weighing the directions according to the assumed probability of intrusion with that angle. The highest probability of conflicts is for the $-\beta$ to β region for both the full and the truncated distribution, however, the peak value for the truncated distribution is less than half of that for the full distribution. Although for small angular deviations from the ownship heading the full distribution probability is greater, for higher angles the truncated distribution takes over.

https://doi.org/10.1017/aer.2023.12 Published online by Cambridge University Press

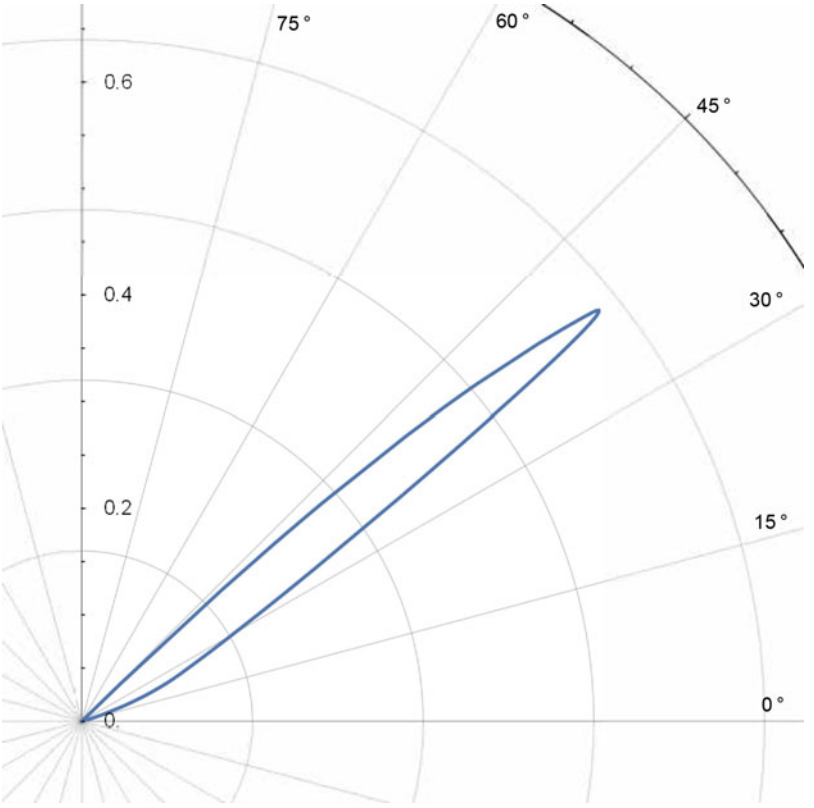

Figure 17. *Polar plot showing the probability of geometric intrusion for $\theta = \frac{\pi}{4}$, truncated exponential distribution with $\rho = 80$ ($a = 0.2$ and $b = 0.0025$, $\theta = \frac{\pi}{4}$, $l = 15$, $u = 180$). The radius coordinate represents conflict probability magnitude, while the angle coordinate shows relative azimuth.*

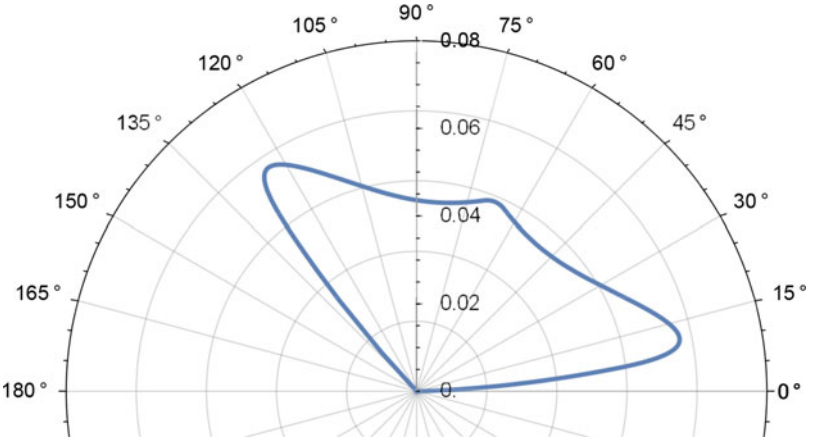

Figure 18. *Polar plot showing the probability of geometric intrusion for $\theta = \frac{3\pi}{4}$, truncated exponential distribution with $\rho = 1$ ($a = 0.0025$ and $b = 0.0025$, $\theta = \frac{3\pi}{4}$, $l = 15$, $u = 180$). The radius coordinate represents conflict probability magnitude, while the angle coordinate shows relative azimuth.*

https://doi.org/10.1017/aer.2023.12 Published online by Cambridge University Press

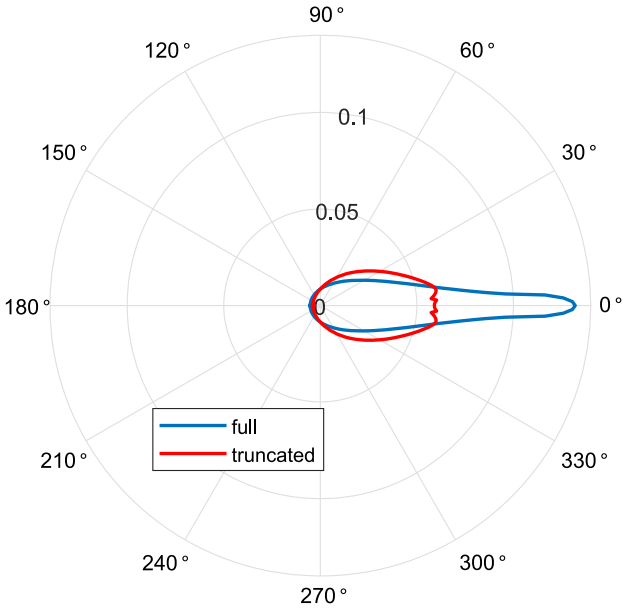

Figure 19. *Polar plot showing the probability of geometric intrusion for full and truncated exponential distribution with $\rho = 1$, averaged over all intrusion angles ($a = 0.0025$ and $b = 0.0025$, $l = 15$, $u = 180$). The radius coordinate represents conflict probability magnitude, while the angle coordinate shows relative azimuth.*

3.6 Probability of entering the conflict range faster than the threshold for perpendicular velocities

Since it is assumed that, provided enough time is available for manoeuvring, collision avoidance methods are able to handle intruders, a conflict emerges only if the traversal from the sensing range to the conflict range is faster than a certain threshold time. This is referred to as a *speed conflict*.

The integrals corresponding to the conflict probabilities cannot be evaluated analytically, however, lower and upper bounds can be given for them based on approximations (Equations (69)–(72), Appendix A.4).

Evaluating the speed conflict limits with a threshold time of $t_{\text{th}} = 60$s provides the speed conflict probability distribution as it can be seen in Figs. 20 and 21. The difference between lower and upper approximations is negligible. Comparing the speed conflict with the geometric conflict probability it can be seen that specifying a time threshold corresponds to a scaling, however with the choice of this threshold time ($t_{\text{th}} = 60$s) the conflict probability does not change very much for the full distribution. The selection of $t_{\text{th}} = 60$s time threshold here is arbitrary for the plots, the formulae can be evaluated for any other parameter. Avoidance logic threshold selection for UAM vehicles in the future would probably be based on classification of airspace, type of operation, vehicle speed and category and CNS performance.

If the set of available speeds is bounded, and thus the distributions are truncated, speed conflict distributions are modified according to Equations (77) (Appendix A.5).

Conflict probabilities for full and truncated exponential distributions for intruders with perpendicular velocities can be seen in Figs. 22 and 23. For high ρ the difference between upper and lower approximations is not so apparent, however, for $\rho = 1$ the effect of the speed threshold is clearly visible.

3.7 Probability of entering the conflict range faster than the threshold for parallel velocities

Speed conflict probabilities can also be calculated for intruder velocities parallel to the ownship velocity. For intruders with velocities pointing in the opposite direction the conflict probability can be calculated

https://doi.org/10.1017/aer.2023.12 Published online by Cambridge University Press

using the formula for the sum of exponentially distributed random variables for a full distribution is given by Equation (47), leading to Equation (33).

$$\Pr_{\text{parallel}}(\text{SC}) = \begin{cases} \dfrac{e^{\frac{-b\,d_{\parallel}(\delta,\beta)}{t_{\text{th}}}}\left(b\,d_{\parallel}(\delta,\beta)+t_{\text{th}}\right)}{t_{\text{th}}} & \text{if } -\beta<\delta<\beta \text{ and } a=b \\ \dfrac{a\,e^{\frac{-b\,d_{\parallel}(\delta,\beta)}{t_{\text{th}}}} - b\,e^{\frac{a\,d_{\parallel}(\delta,\beta)}{t_{\text{th}}}}}{a-b} & \text{if } -\beta<\delta<\beta \text{ and } a\neq b \\ 0 & \text{if } \delta\leq-\beta \text{ or } \beta\leq\delta \end{cases} \tag{33}$$

If distributions are truncated, the sum of exponentially distributed random variables is given by Equation (51), thus speed conflict probability becomes Equation (34).

$$\Pr_{\text{parallel}}(\text{SC}') = \begin{cases} \dfrac{e^{2au}\left(2al-\frac{ad_{\parallel}(\delta,\beta)}{t_{\text{th}}}-1\right)}{\left(e^{al}-e^{au}\right)^2}\dfrac{\exp\left(2al-\frac{ad_{\parallel}(\delta,\beta)}{t_{\text{th}}}\right)}{\left(e^{al}-e^{au}\right)^2}+\dfrac{e^{2au}}{\left(e^{al}-e^{au}\right)^2} & \text{if } l+u\geq\dfrac{d(\delta,\gamma)}{t_{\text{th}}} \text{ and } a=b \text{ and} \\ & 2l\leq\dfrac{d(\delta,\gamma)}{t_{\text{th}}}\leq 2u \text{ and } -\beta<\delta<\beta \\ \dfrac{1}{\left(e^{al}-e^{au}\right)^2} & \text{if } l+u\leq\dfrac{d(\delta,\gamma)}{t_{\text{th}}} \text{ and } a=b \text{ and} \\ & 2l\leq\dfrac{d(\delta,\gamma)}{t_{\text{th}}}\leq 2u \text{ and } -\beta<\delta<\beta \\ \dfrac{a\exp\left(al+b\left(l-\frac{d_{\parallel}(\delta,\beta)}{t_{\text{th}}}+2u\right)\right)}{(a-b)\left(e^{al}-e^{au}\right)\left(e^{bl}-e^{bu}\right)}-\dfrac{a\left(e^{au+bl}-e^{al+bu}+e^{u(a+b)}\right)}{(a-b)\left(e^{al}-e^{au}\right)\left(e^{bl}-e^{bu}\right)} & \\ -\dfrac{b\exp\left(a\left(l-\frac{d_{\parallel}(\delta,\beta)}{t_{\text{th}}}+2u\right)+bl\right)}{(a-b)\left(e^{al}-e^{au}\right)\left(e^{bl}-e^{bu}\right)}-\dfrac{b\left(e^{au+bl}-e^{al+bu}+e^{u(a+b)}\right)}{(a-b)\left(e^{al}-e^{au}\right)\left(e^{bl}-e^{bu}\right)} & \text{if } l+u\geq\dfrac{d(\delta,\gamma)}{t_{\text{th}}} \text{ and } a\neq b \text{ and} \\ & 2l\leq\dfrac{d(\delta,\gamma)}{t_{\text{th}}}\leq 2u \text{ and } -\beta<\delta<\beta \\ \dfrac{\left(a\,e^{u(a+b)}\left(-\exp\left(2bl-\frac{bd_{\parallel}(\delta,\beta)}{t_{\text{th}}}\right)\right)\right)}{(a-b)\left(e^{al}-e^{au}\right)\left(e^{bl}-e^{bu}\right)} & \\ +\dfrac{be^{u(a+b)}\left(\exp\left(2al-\frac{ad_{\parallel}(\delta,\beta)}{t_{\text{th}}}\right)-1\right)+ae^{u(a+b)}}{(a-b)\left(e^{al}-e^{au}\right)\left(e^{bl}-e^{bu}\right)} & \text{if } l+u\leq\dfrac{d(\delta,\gamma)}{t_{\text{th}}} \text{ and } a\neq b \text{ and} \\ & 2l\leq\dfrac{d(\delta,\gamma)}{t_{\text{th}}}\leq 2u \text{ and } -\beta<\delta<\beta \\ 0 & \text{if } 2l>\dfrac{d(\delta,\gamma)}{t_{\text{th}}} \text{ and } -\beta<\delta<\beta \\ 1 & \text{if } 2u<\dfrac{d(\delta,\gamma)}{t_{\text{th}}} \text{ and } -\beta<\delta<\beta \\ 0 & \text{if } \delta\leq-\beta \text{ or } \beta\leq\delta \end{cases} \tag{34}$$

https://doi.org/10.1017/aer.2023.12 Published online by Cambridge University Press

For intruders having a velocity with the same direction the probability of a speed conflict can be calculated according to Equations (35) for full and Equation (36) for truncated distributions.

$$\Pr_{\text{parallel}}(\text{SC}) = \begin{cases} \dfrac{b\, e^{\frac{a\, r_S\left(\sqrt{\cos^2(\delta)-\cos^2(\beta)}+\cos(\delta)\right)}{t_{\text{th}}}}}{a+b} & \text{if } \delta < -\pi+\beta \text{ or } \pi-\beta < \delta \\ 1-\dfrac{b\, e^{\frac{a\, r_S\left(\sqrt{\cos^2(\delta)-\cos^2(\beta)}+\cos(\delta)\right)}{t_{\text{th}}}}}{a+b} & \text{if } -\beta < \delta < \beta \\ 0 & \text{if } -\pi+\beta \le \delta \le \pi-\beta \end{cases} \tag{35}$$

$$\Pr_{\text{parallel}}(\text{SC}') = \begin{cases} 0 & \text{if } u-l < \dfrac{d(\delta,\gamma)}{t_{\text{th}}} \text{ and } (\delta < -\pi+\beta \text{ or } \pi-\beta < \delta) \\ 1-\dfrac{a\left(-\exp\left(al+bl-\dfrac{br_S\sqrt{\cos(2\delta)-\cos(2\beta)}}{\sqrt{2}t_{\text{th}}}-\dfrac{br_S\cos(\delta)}{t_{\text{th}}}\right)-e^{au+bl}+e^{l(a+b)}+e^{u(a+b)}\right)}{(a+b)\left(e^{al}-e^{au}\right)\left(e^{bl}-e^{bu}\right)} \\ \quad -\dfrac{b\left(-\exp\left(u(a+b)+\dfrac{ar_S\left(\sqrt{\cos^2(\delta)-\cos^2(\beta)}+\cos(\delta)\right)}{t_{\text{th}}}\right)-e^{au+bl}+e^{l(a+b)}+e^{u(a+b)}\right)}{(a+b)\left(e^{al}-e^{au}\right)\left(e^{bl}-e^{bu}\right)} & \text{if } u-l \ge \dfrac{d(\delta,\gamma)}{t_{\text{th}}} \text{ and } (\delta < -\pi+\beta \text{ or } \pi-\beta < \delta) \\ 0 & \text{if } u-l < \dfrac{d(\delta,\gamma)}{t_{\text{th}}} \text{ and } -\beta < \delta < \beta \\ \dfrac{a\left(-\exp\left(al+bl-\dfrac{br_S\sqrt{\cos(2\delta)-\cos(2\beta)}}{\sqrt{2}t_{\text{th}}}-\dfrac{br_S\cos(\delta)}{t_{\text{th}}}\right)-e^{au+bl}+e^{l(a+b)}+e^{u(a+b)}\right)}{(a+b)\left(e^{al}-e^{au}\right)\left(e^{bl}-e^{bu}\right)} \\ \quad +\dfrac{b\left(-\exp\left(u(a+b)+\dfrac{ar_S\left(\sqrt{\cos^2(\delta)-\cos^2(\beta)}+\cos(\delta)\right)}{t_{\text{th}}}\right)-e^{au+bl}+e^{l(a+b)}+e^{u(a+b)}\right)}{(a+b)\left(e^{al}-e^{au}\right)\left(e^{bl}-e^{bu}\right)} & \text{if } u-l \ge \dfrac{d(\delta,\gamma)}{t_{\text{th}}} \text{ and } -\beta < \delta < \beta \\ 0 & \text{if } -\pi+\beta \le \delta \le \pi-\beta \end{cases} \tag{36}$$

3.8 Probability of entering the conflict range faster than the threshold for velocities with arbitrary direction

The speed conflict probability for intruders with arbitrary velocity directions was also analysed. Calculations were performed according to sections of the intruder velocity angle and can be found in Appendix A.6.

https://doi.org/10.1017/aer.2023.12 Published online by Cambridge University Press

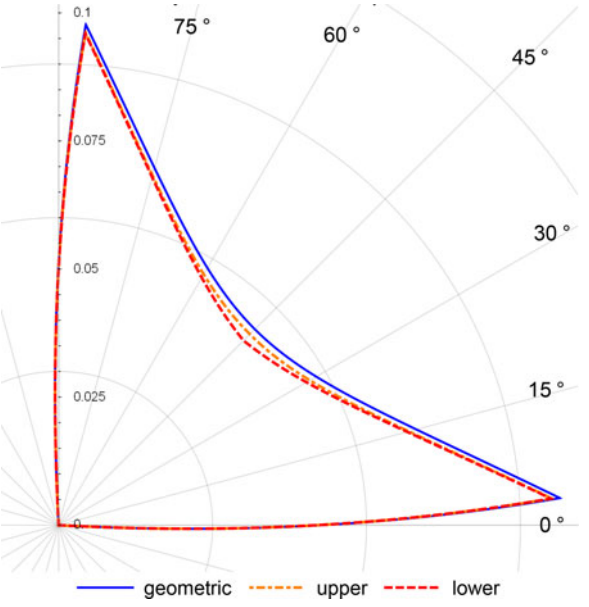

Figure 20. *Polar plot showing the upper and lower bounds for probability of speed intrusion, exponential distribution with* $\rho = 1$*, perpendicular intruder velocity (*$a = 0.0025$ *and* $b = 0.0025$*,* $\theta = \frac{\pi}{2}$*,* $t_{\text{th}} = 60$*). The radius coordinate represents conflict probability magnitude, while the angle coordinate shows relative azimuth.*

Assuming a truncated distribution the conflict probabilities can be calculated similarly, the range of θ is sectioned according to Equation (37).

$$\begin{gathered} -\beta < \delta \leq \beta \text{ and } \theta = 0 \\ 0 < \theta \leq 2\beta \\ 2\beta < \theta \leq 4\beta \\ 4\beta < \theta \leq \tfrac{\pi}{2} \\ \frac{\pi}{2} < \theta \leq \pi \end{gathered} \tag{37}$$

Evaluating the integrals leads to the results shown in Fig. 24 for $\theta = \pi/4$ and Fig. 25 for $\theta = 3\pi/4$. Once again the effect of changing the intruder velocity direction can be seen (central angular scaling), together with the effect of truncation, and how the difference between upper and lower approximations for truncated distributions is more conspicuous.

4.0 Calculations for normal distribution

As stated in Section 3, conflict probabilities can be calculated for any desired distribution using the presented chain of deduction and integration limits. As normal speed distribution is representative of a perturbed traffic flow, making it another sensible example, the same procedure was performed for normal prescribed speed distributions. In this section, only the major differences worth highlighting are summarised.

The parameter ranges and speed limits used for normal distribution are given in Equations (38)–(40).

$$\mu \in [5, 90]\,, \nu \in [5, 90] \tag{38}$$

https://doi.org/10.1017/aer.2023.12 Published online by Cambridge University Press

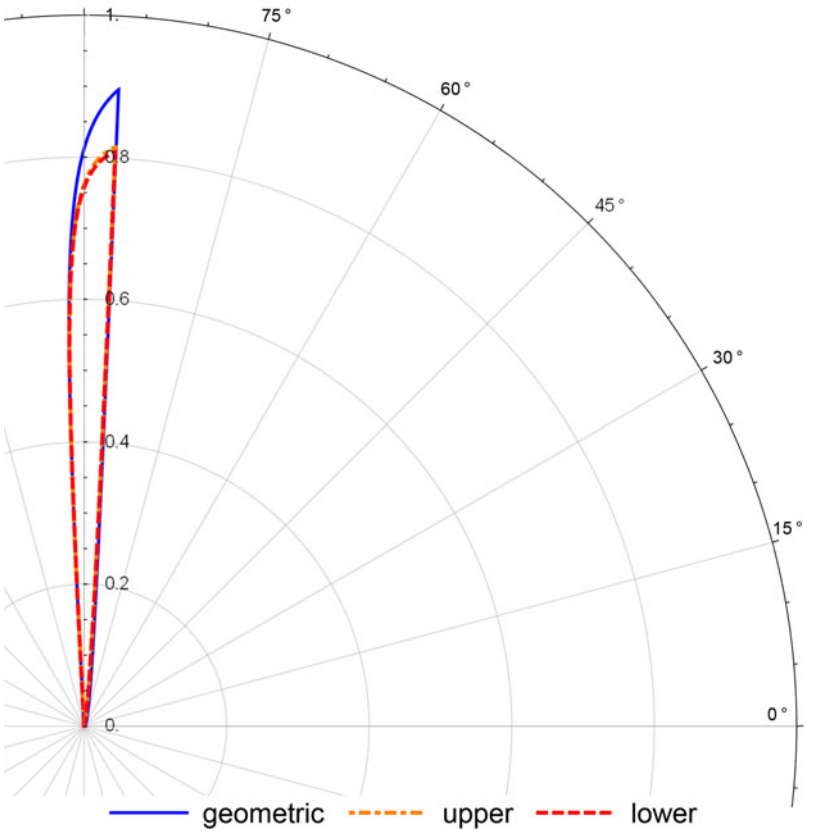

Figure 21. *Polar plot showing the upper and lower bounds for probability of speed intrusion, exponential distribution with $\rho = 80$, perpendicular intruder velocity ($a = 0.2$ and $b = 0.0025$, $\theta = \frac{\pi}{2}$, $t_{\text{th}} = 60$). The radius coordinate represents conflict probability magnitude, while the angle coordinate shows relative azimuth.*

$$l = 15 \text{ [knots]} \tag{39}$$

$$u = 180 \text{ [knots]} \tag{40}$$

The mean speeds for the chosen parameter range and speed limits for the truncated normal distribution are shown in Fig. 26. Generally, higher values of the location parameter (μ or ν) indicate higher mean speeds.

For the probability density function of the ratio of normal variables the approximation given by Equation (41) and (42) is used, according to Hayya, Armstrong and Gressis [48].

$$f_{\frac{x}{y}}(x, y; \mu, \nu) \approx \frac{e^{-\frac{(\mu - \nu z)^2}{2\left(\sigma_x^2 + \sigma_y^2 z^2\right)}} \left(\nu \sigma_x^2 + \mu \sigma_y^2 z\right)}{\sqrt{2\pi}\left(\sigma_x^2 + \sigma_y^2 z^2\right)^{3/2}} \tag{41}$$

$$F_{\frac{x}{y}}(x, y; \mu, \nu) \approx \frac{1}{2}\text{erfc}\left(-\frac{\nu z - \mu}{\sqrt{2}\sqrt{\sigma_x^2 + \sigma_y^2 z^2}}\right) \tag{42}$$

The exact functions can be found in the papers by Hinkley [49] and Cedilnik, Košmelj and Blejec [50]. Both formulae were compared to the approximation and each other, and the difference was found to be negligible.

https://doi.org/10.1017/aer.2023.12 Published online by Cambridge University Press

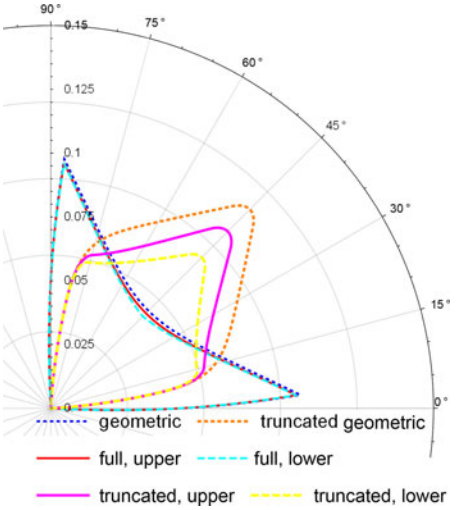

Figure 22. *Polar plot showing the upper and lower bounds for probability of speed intrusion, full and truncated exponential distribution with* $\rho = 1$*, perpendicular intruder velocity (*$a = 0.0025$ *and* $b = 0.0025$*,* $\theta = \frac{\pi}{2}$*,* $t_{\text{th}} = 60$*). The radius coordinate represents conflict probability magnitude, while the angle coordinate shows relative azimuth.*

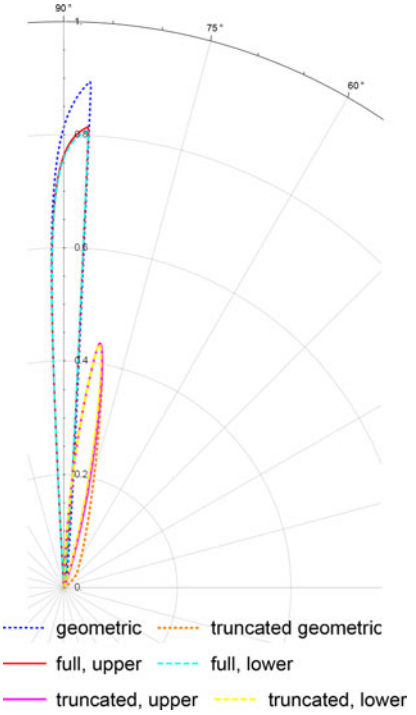

Figure 23. *Polar plot showing the upper and lower bounds for probability of speed intrusion, full and truncated exponential distribution with* $\rho = 80$*, perpendicular intruder velocity (*$a = 0.2$ *and* $b = 0.0025$*,* $\theta = \frac{\pi}{2}$*,* $t_{\text{th}} = 60$*). The radius coordinate represents conflict probability magnitude, while the angle coordinate shows relative azimuth.*

https://doi.org/10.1017/aer.2023.12 Published online by Cambridge University Press

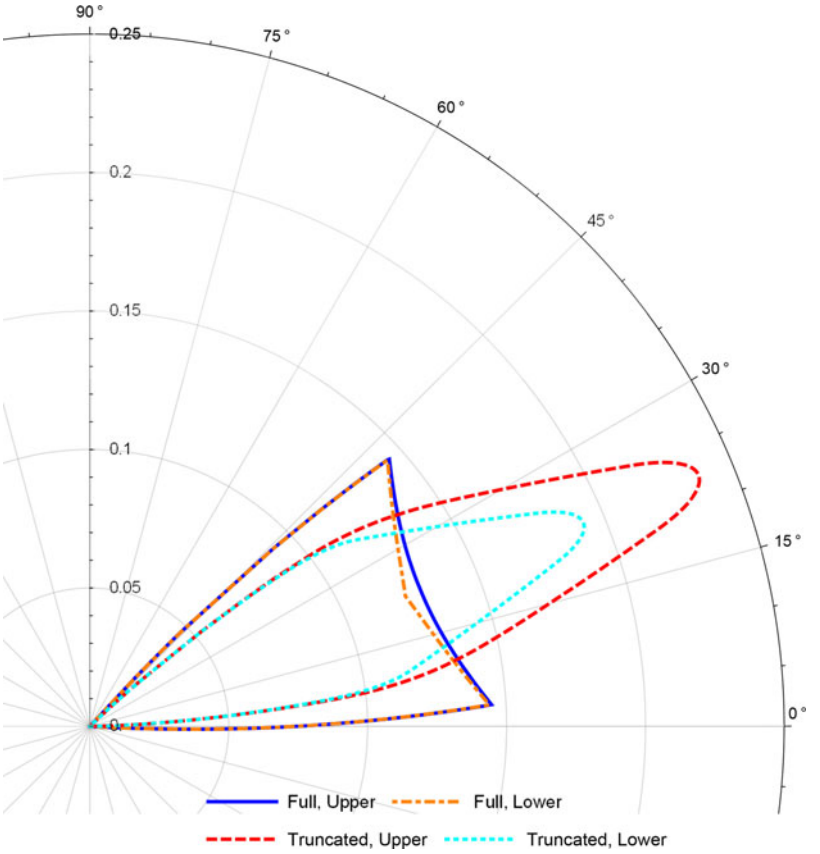

Figure 24. *Polar plot showing the upper and lower bounds for probability of speed intrusion, full and truncated exponential distribution with* $\rho = 1$*, intruder velocity angle* $\frac{\pi}{4}$ *(*$a = 0.0025$ *and* $b = 0.0025$*,* $\theta = \frac{\pi}{4}$*,* $t_{\text{th}} = 60$*). The radius coordinate represents conflict probability magnitude, while the angle coordinate shows relative azimuth.*

To be able to calculate conflict probabilities for truncated distributions and to handle speed conflicts the joint probability distribution for x and y was written in terms of p and q defined according to Equation (43).

$$p = \sqrt{x^2 + y^2}$$
$$q = \frac{x}{y} \tag{43}$$

By completing the squares the joint probability distribution function can be written as a product of the PDF of p (dependent of q) and a scaling term containing q only, as elaborated in Appendix B.1. The integral for p can thus be analytically evaluated. Conflict calculation results are shown in Figs. 27 and 28.

Averaging for all possible intrusion angles yields the results in Fig. 29. As opposed to the exponential distribution, which has its maximum in the $-\beta$ to β region for normal distribution the maximum is at $\frac{11}{40}\pi$. Compared to the exponential distribution the range of angles with similar corresponding magnitudes is much wider (around 0.8π for normal distribution as opposed to around 0.3π for exponential distribution), however, the probability magnitudes are generally lower. The difference between the full and truncated distribution is not significant.

https://doi.org/10.1017/aer.2023.12 Published online by Cambridge University Press

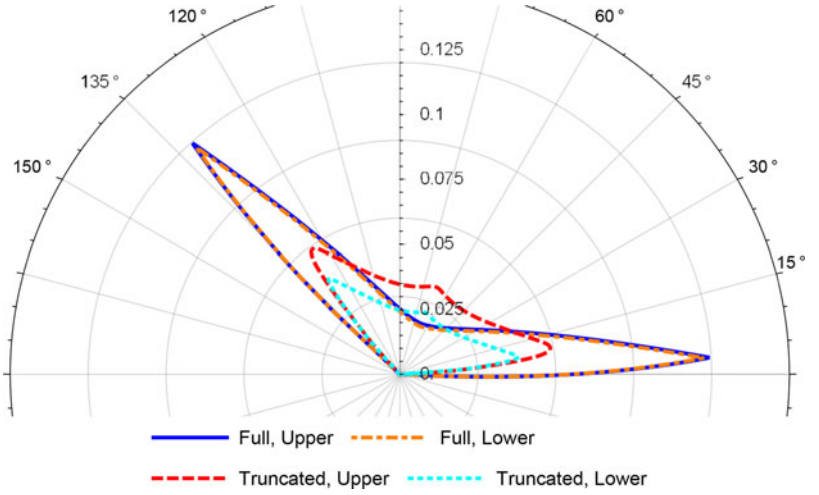

Figure 25. *Polar plot showing the upper and lower bounds for probability of speed intrusion, full and truncated exponential distribution with* $\rho = 1$*, intruder velocity angle* $\frac{3\pi}{4}$ *(*$a = 0.0025$ *and* $b = 0.0025$*,* $\theta = \frac{3\pi}{4}$*,* $t_{\text{th}} = 60$*). The radius coordinate represents conflict probability magnitude, while the angle coordinate shows relative azimuth.*

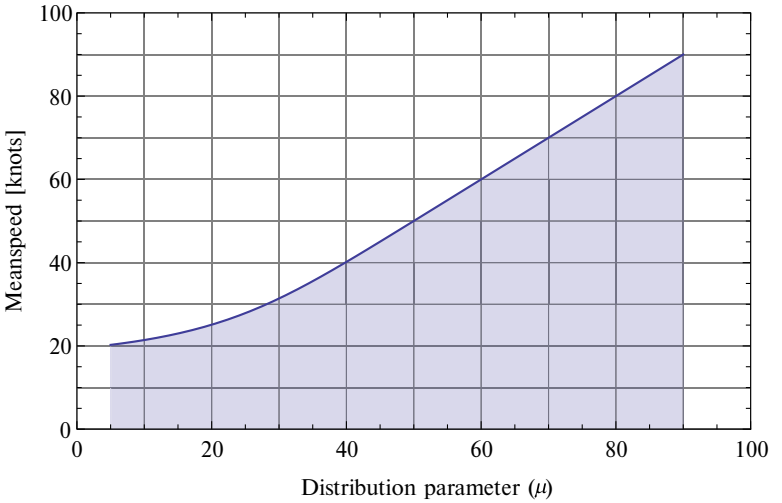

Figure 26. *Mean speed in Kn as a function of the normal distribution parameter (*μ *for the ownship and* ν *for the intruder).*

Calculations can be performed for any mean and standard deviation. Changing the standard deviation can help represent the heterogeneity of vehicles, which the exponential distribution cannot represent because it has only a single parameter. For normal distributions, it was found that changing the standard deviation does not alter the principal shape of the results, but it spreads the conflict probabilities widening the angles affected and decreasing the peak magnitude (Fig. 30). The total conflict probability does not change with varying the standard deviation.

It is also possible to calculate conflict probabilities for mismatched standard deviations. If standard deviations are not equal, the conflict probability map becomes distorted, as it can be seen in Fig. 31.

https://doi.org/10.1017/aer.2023.12 Published online by Cambridge University Press

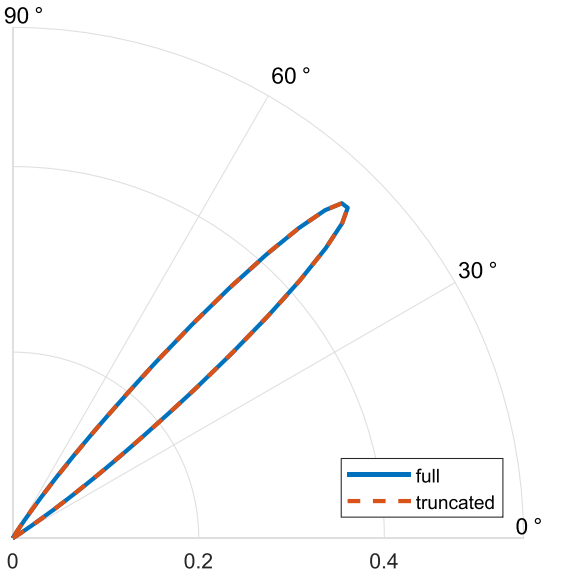

Figure 27. *Polar plot showing the probability of geometric intrusion with perpendicular intruder velocity for full and truncated normal distribution with* $\rho = 1$ *(*$\mu = 90$ *and* $\nu = 90$*,* $\sigma_x = 10$*,* $\sigma_y = 10$*,* $\theta = \frac{\pi}{2}$*,* $l = 15$*,* $u = 180$*). The radius coordinate represents conflict probability magnitude, while the angle coordinate shows relative azimuth.*

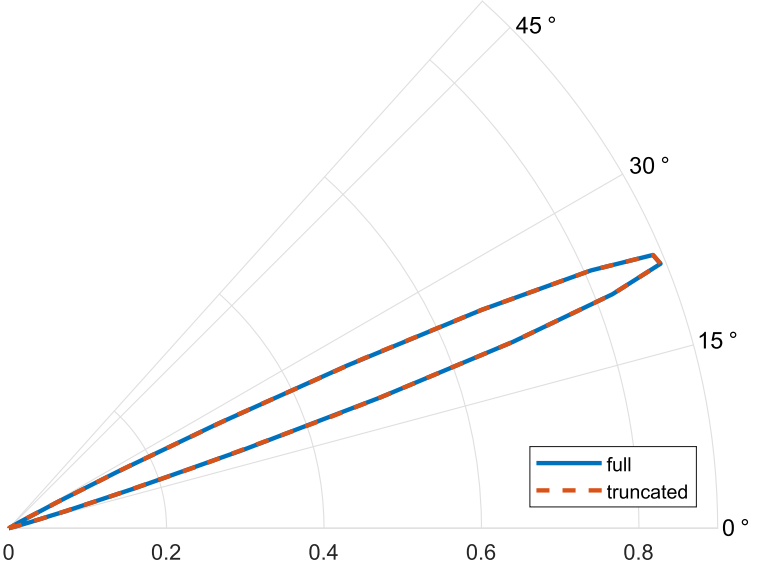

Figure 28. *Polar plot showing the probability of geometric intrusion with intruder velocity angle* $\pi/4$ *for full and truncated normal distribution with* $\rho = 1$ *(*$\mu = 90$ *and* $\nu = 90$*,* $\sigma_x = 10$*,* $\sigma_y = 10$*,* $\theta = \frac{\pi}{4}$*,* $l = 15$*,* $u = 180$*). The radius coordinate represents conflict probability magnitude, while the angle coordinate shows relative azimuth.*

https://doi.org/10.1017/aer.2023.12 Published online by Cambridge University Press

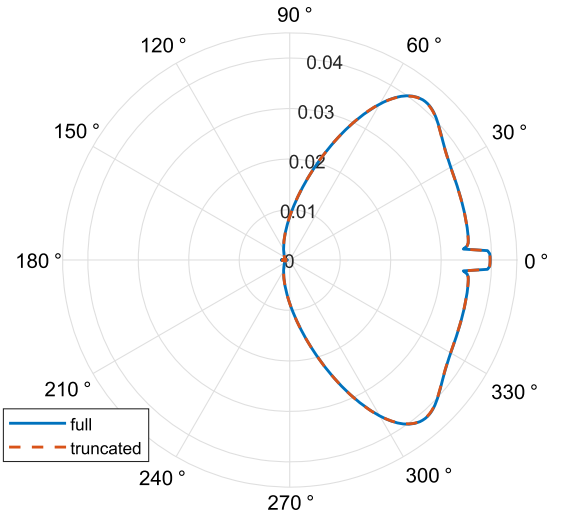

Figure 29. *Polar plot showing the probability of geometric intrusion averaged over all possible intruder heading angles for full and truncated normal distribution with* $\rho = 1$ *(*$\mu = 90$ *and* $v = 90$*,* $\sigma_x = 10$*,* $\sigma_y = 10$*,* $l = 15$*,* $u = 180$*). The radius coordinate represents conflict probability magnitude, while the angle coordinate shows relative azimuth.*

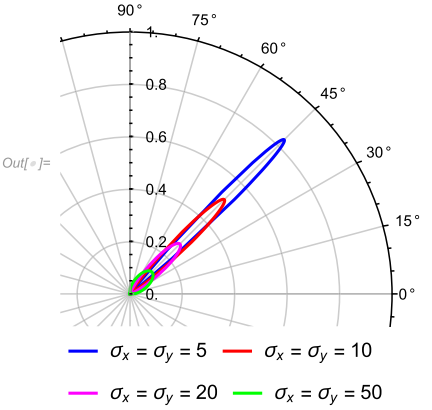

Figure 30. *Polar plot showing the probability of geometric intrusion for perpendicular velocities for full normal distribution with* $\rho = 1$ *(*$\mu = 90$ *and* $v = 90$*,* $l = 15$*,* $u = 180$*) for a range of equal standard deviations. The radius coordinate represents conflict probability magnitude, while the angle coordinate shows relative azimuth.*

Since the standard deviation of the normal distribution is not considered to be a decision variable, for the remaining part of the paper it is set as $\sigma_x = \sigma_y = 10$.

5.0 Verification of calculations using numerical simulations

The calculations were verified using Monte-Carlo simulations. After discretising the set of possible intrusion angles and relative headings, conflict probability was calculated for each angle of the discrete set as the ratio of samples resulting in a conflict divided by the total number of samples for a particular intrusion angle. A sample of speeds according to the prescribed distribution was generated by inverse

https://doi.org/10.1017/aer.2023.12 Published online by Cambridge University Press

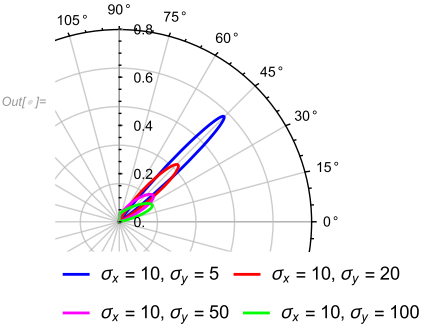

Figure 31. *Polar plot showing the probability of geometric intrusion for perpendicular velocities for full normal distribution with $\rho = 1$ ($\mu = 90$ and $v = 90$, $l = 15$, $u = 180$) for a range of mismatched standard deviations. The radius coordinate represents conflict probability magnitude, while the angle coordinate shows relative azimuth.*

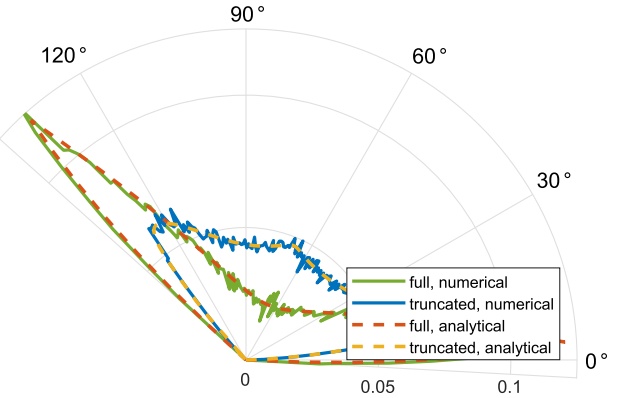

Figure 32. *Polar plot showing the probability of geometric intrusion with intruder velocity angle $3\pi/4$ for full and truncated exponential distribution with $\rho = 1$ – comparison of analytical and numerical results ($a = 0.0025$ and $b = 0.0025$, $\theta = \frac{3\pi}{4}$, $l = 15$, $u = 180$). The radius coordinate represents conflict probability magnitude, while the angle coordinate shows relative azimuth.*

transform sampling. Using inverse transform sampling, a sample of uniformly distributed variables is transformed according to the cumulative distribution function of the desired sample distribution [51]. Given all the parameters (intrusion angle, ownship speed, intruder speed, relative heading) the angle of the apparent path and the distance and time traversed can be calculated (Equation (29), (6) and $t = d/v_{\text{res}}$ respectively), which, according to the definitions determine whether a conflict occurs or not. Resultant speed (v_{res}) is calculated by projecting both velocities to the apparent path, as in Equation (44).

$$v_{\text{res}} = v_{\text{O}} \sin \Omega + v_{\text{I}} \sin(\theta + \Omega) \tag{44}$$

Comparing the number of conflict occurrences to the sample size provides the conflict probability for a given angle pair.

The comparison of analytical and numerical results is shown in Fig. 32 for exponential distribution and Fig. 33 for normal distribution. Apart from the fluctuations typical for numerical methods the results are in agreement, verifying the analytical formulae.

Numerical simulations were also used to evaluate the robustness of estimations. Speed distributions and the intrusion angle were perturbed by adding zero-mean normally distributed noise to the sampled

https://doi.org/10.1017/aer.2023.12 Published online by Cambridge University Press

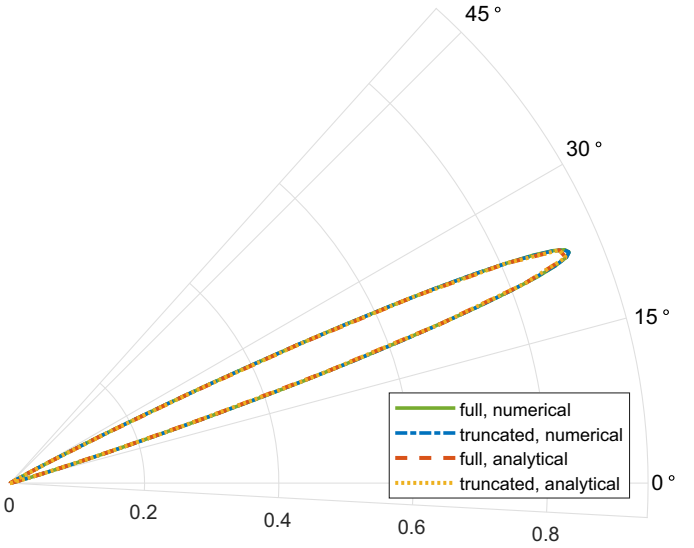

Figure 33. *Polar plot showing the probability of geometric intrusion with intruder velocity angle $\pi/4$ for full and truncated normal distribution with $\rho = 1$ – comparison of analytical and numerical results ($\mu = 90$ and $v = 90$, $\sigma_x = 10$, $\sigma_y = 10$, $\theta = \frac{\pi}{4}$, $l = 15$, $u = 180$). The radius coordinate represents conflict probability magnitude, while the angle coordinate shows relative azimuth.*

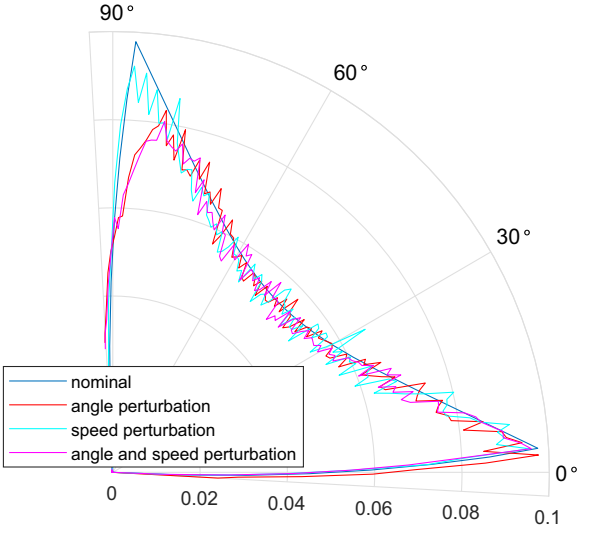

Figure 34. *Polar plot showing the probability of geometric intrusion with perpendicular intruder velocity for exponential distribution with $\rho = 1$ – comparison of perturbed and nominal simulations ($a = 0.0025$ and $b = 0.0025$, $\theta = \frac{\pi}{2}$, $\sigma_v = 10$, $\sigma_\theta = 5°$). The radius coordinate represents conflict probability magnitude, while the angle coordinate shows relative azimuth.*

https://doi.org/10.1017/aer.2023.12 Published online by Cambridge University Press

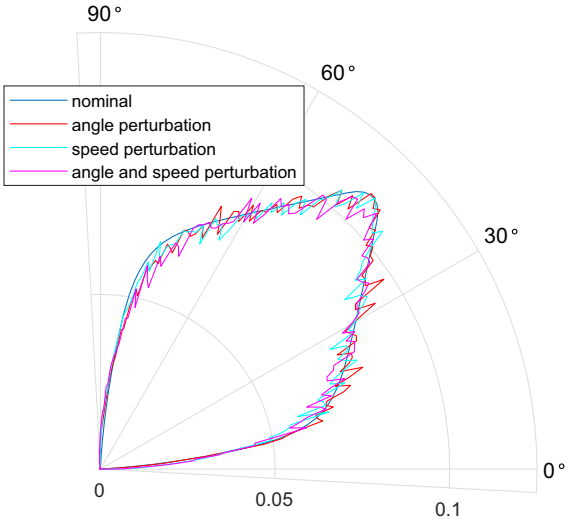

Figure 35. *Polar plot showing the probability of geometric intrusion with perpendicular intruder velocity for truncated exponential distribution with $\rho = 1$ – comparison of perturbed and nominal simulations ($a = 0.0025$ and $b = 0.0025$, $\theta = \frac{\pi}{2}$, $l = 15$, $u = 180$, $\sigma_v = 10$, $\sigma_\theta = 5°$). The radius coordinate represents conflict probability magnitude, while the angle coordinate shows relative azimuth.*

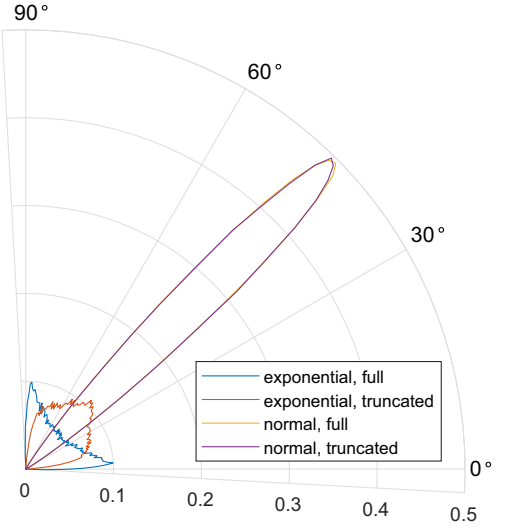

Figure 36. *Polar plot showing the probability of geometric intrusion with perpendicular intrusion angle for full and truncated exponential and normal distributions with $\rho = 1$ – comparison of results for distributions with matching mean speeds ($a = 0.00422$ and $b = 0.00422$, $\mu = 88$, $v = 88$, $\sigma_x = 10$, $\sigma_y = 10$, $\theta = \frac{\pi}{2}$, $l = 15$, $u = 180$). The radius coordinate represents conflict probability magnitude, while the angle coordinate shows relative azimuth.*

https://doi.org/10.1017/aer.2023.12 Published online by Cambridge University Press

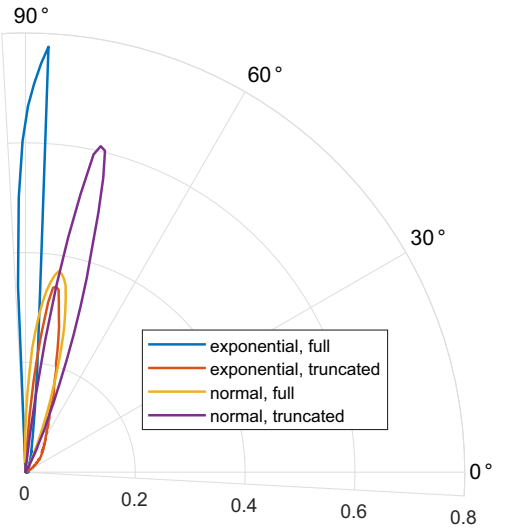

Figure 37. *Polar plot showing the probability of geometric intrusion with perpendicular intrusion angle for full and truncated exponential and normal distributions – comparison of results for distributions with matching mean speeds ($a = 0.125$ and $b = 0.00422$, $\mu = 15$, $\nu = 88$, $\sigma_x = 10$, $\sigma_y = 10$, $\theta = \frac{\pi}{2}$, $l = 15$, $u = 180$). The radius coordinate represents conflict probability magnitude, while the angle coordinate shows relative azimuth.*

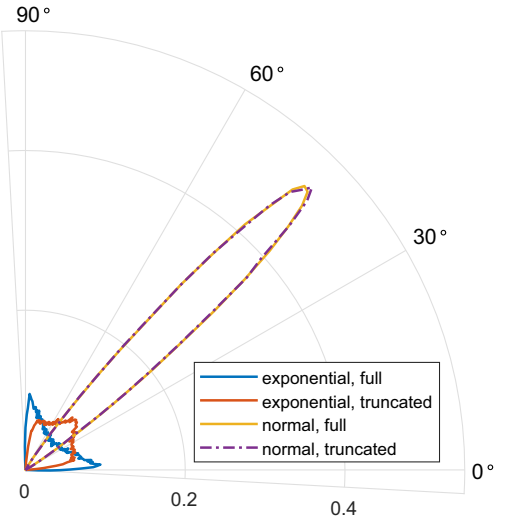

Figure 38. *Polar plot showing the probability of speed intrusion with perpendicular intrusion angle for full and truncated exponential and normal distributions – comparison of results for distributions with matching mean speeds ($a = 0.00422$ and $b = 0.00422$, $\mu = 88$, $\nu = 88$, $\sigma_x = 10$, $\sigma_y = 10$, $\theta = \frac{\pi}{2}$, $l = 15$, $u = 180$). The radius coordinate represents conflict probability magnitude, while the angle coordinate shows relative azimuth.*

https://doi.org/10.1017/aer.2023.12 Published online by Cambridge University Press

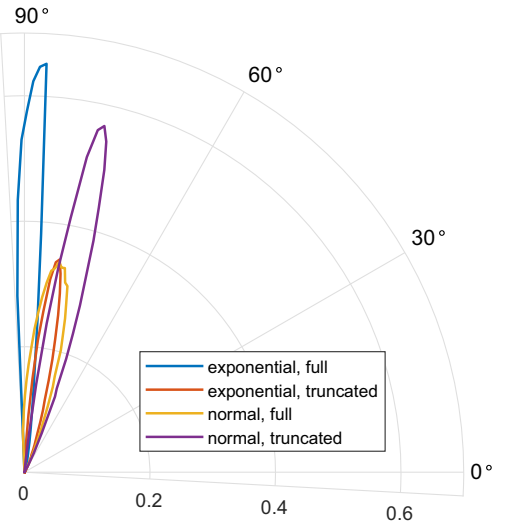

Figure 39. *Polar plot showing the probability of speed intrusion with perpendicular intrusion angle for full and truncated exponential and normal distributions – comparison of results for distributions with matching mean speeds ($a = 0.125$ and $b = 0.00422$, $\mu = 15$, $\nu = 88$, $\sigma_x = 10$, $\sigma_y = 10$, $\theta = \frac{\pi}{2}$, $l = 15$, $u = 180$). The radius coordinate represents conflict probability magnitude, while the angle coordinate shows relative azimuth.*

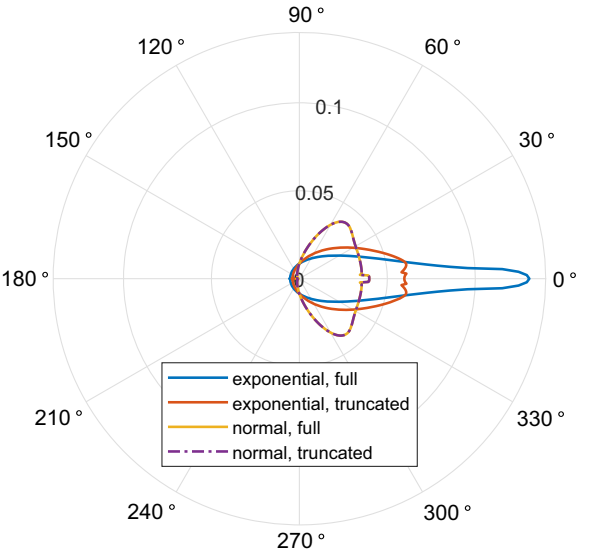

Figure 40. *Polar plot showing the probability of speed intrusion averaged over possible intrusion angles for full and truncated exponential and normal distributions – comparison of results for distributions with matching mean speeds ($a = 0.00422$ and $b = 0.00422$, $\mu = 88$, $\nu = 88$, $\sigma_x = 10$, $\sigma_y = 10$, $l = 15$, $u = 180$). The radius coordinate represents conflict probability magnitude, while the angle coordinate shows relative azimuth.*

https://doi.org/10.1017/aer.2023.12 Published online by Cambridge University Press

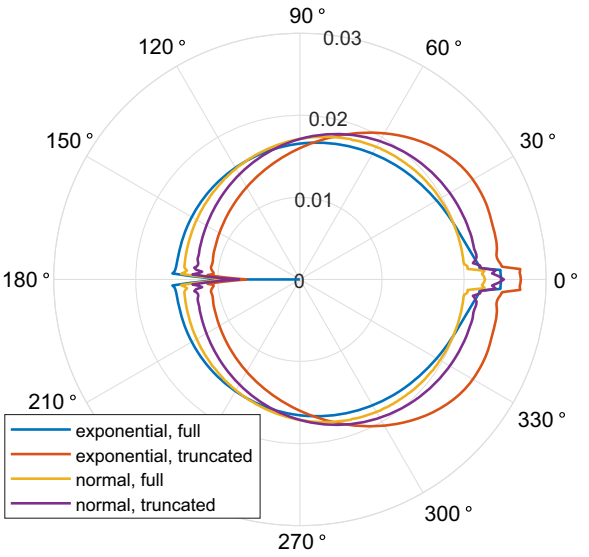

Figure 41. *Polar plot showing the probability of speed intrusion averaged over possible intrusion angles for full and truncated exponential and normal distributions – comparison of results for distributions with matching mean speeds ($a = 0.125$ and $b = 0.00422$, $\mu = 15$, $\nu = 88$, $\sigma_x = 10$, $\sigma_y = 10$, $l = 15$, $u = 180$). The radius coordinate represents conflict probability magnitude, while the angle coordinate shows relative azimuth.*

speed and heading values with the given deviations ($\sigma_v = 10$, $\sigma_\theta = 5°$), and results are compared to nominal simulations. Perturbations may be considered analogous to navigation uncertainties. Depending on equipage, vehicles can be categorised in terms of these uncertainties. The categories are also broadcast via ADS-B [52]. Further standardisation of equipage and performance for UASs and UAM is highly likely. Comparisons for perpendicular intrusions with exponential distributions are shown in Figs. 34 and 35. For full distributions perturbation of speed does not modify conflict probability significantly, the angle perturbation however decreases the peak probability. In case of truncated distributions, no significant change can be seen.

6.0 Analysis of results

In this section characteristics of the conflict probabilities are analysed and compared for exponential and normal prescribed distributions. This comparative analysis can form the basis of the selection of the desired distribution for different traffic scenarios.

For an intruder arriving from the perpendicular direction the range of angles that might lead to conflicts is much wider for exponential than for normal distribution. Especially for full distribution, while the corresponding probabilities are smaller, the overall conflict probability is the same, and independent of the type of distribution (Figs. 36 and 37). For unequal parameters, the range of possible conflict angles shrinks for all distributions, being wider for normal distribution with lower amplitudes. Changing the parameters of distributions only changes the angular distribution, not the overall probability of a conflict. The same characteristics can be seen for speed conflicts, with the threshold time of $t_{\text{th}} = 60$ s the trends are generally the same (Figs. 38 and 39).

The overall conflict probability stays the same when calculated for all headings. Similarly to the perpendicular case, the angle range is wider for the normal distribution and the probabilities are lower. For unequal parameters, the difference becomes less, and the shape of the distributions become similar (Figs. 40 and 41).

https://doi.org/10.1017/aer.2023.12 Published online by Cambridge University Press

7.0 Conclusions

7.1 Summary

In this paper, the conflict situation was analysed with speed distributions for both the ownship and the intruder. Exponential and normal distributions were assumed, both in their full form and with truncation to account for the limited range of achievable speeds. Analytical formulae were derived for conflict probability, at first for perpendicular and parallel intrusions, which were then extended for arbitrary angles intrusions. Assuming a uniform probability for intrusion angles conflict probabilities were averaged. Results were verified using numerical (Monte Carlo) simulations. The sensitivity of results to parameter variations was calculated and simulated, results showed perturbations have no significant effect.

Calculation outcomes lead to the following findings. Truncating the distribution of possible speeds has a significant effect on conflict probability distribution in the exponential case, however, for normal distribution, the effect is almost negligible. For geometric conflicts, only the shape of the distribution is affected by changing the parameters. The overall conflict probability stays the same, similarly to the waterbed effect. For speed conflicts, however, the overall probability can also be modified by the choice of parameters. One of the key points of progress is that formulae for conflict probabilities were calculated, thus the exact relationship is known. A significant drawback of the results is the complexity of expressions, therefore to be applicable for conflict resolution appropriate approximations need to be found.

7.2 Future work

Future work includes the integration of the derived formulae into the optimisation part of the proposed framework, together with the analysis of the effect of distribution shaping when applied in concert with heading-based altitude separation. The method can also be extended to three dimensions, taking into account climbing and descending as well. Another extension would be to investigate the transformation of conflict probabilities when an avoidance manoeuvre is applied and formulate a conflict resolution algorithm for the low layer of the framework. Also, the synthesis of the ideal behaviour distribution holds significant merit.

Acknowledgements. The authors gratefully acknowledge that this research was supported by the Engineering and Physical Sciences Research Council, under grant EPSRC EP/N509450/1.

The authors confirm that the data supporting the findings of this study are available within the paper and its supplementary materials.

Raw data is available from the corresponding author, Zs. Ö., upon reasonable request. The authors declared no potential conflicts of interest with respect to the research, authorship, and/or publication of this paper.

References

[1] Macrina, G., Pugliese, L.D.P., Guerriero, F. and Laporte, G. Drone-aided routing: A literature review, *Transp Res C: Emer Technol*, **120**, 2020, https://doi.org/10.1016/j.trc.2020.102762.

[2] Kopardekar, P.H. Unmanned aerial system (UAS) traffic management (UTM): Enabling low-altitude airspace and UAS operations. NASA/TM-2014-218299, 2014.

[3] Vascik, P.D. and Hansman, R.J. Scaling Constraints for Urban Air Mobility Operations: Air Traffic Control, Ground Infrastructure, and Noise, 2018 Aviation Technology, Integration, and Operations Conference, 2018, https://doi.org/10.2514/6.2018-3849.

[4] Thipphavong, D.P., Apaza, R., Barmore, B., Battiste, V., Burian, B., Dao, Q., Feary, M., Go, S., Goodrich, K.H., Homola, J., Idris, H.R., Kopardekar, P.H., Lachter, J.B., Neogi, N.A., Ng, H.K., Oseguera-Lohr, R.M., Patterson, M.D. and Verma S.A. Urban Air Mobility Airspace Integration Concepts and Considerations, AIAA Aviation Forum (Aviation 2018), June 25, 2018 – June 29, 2018; Atlanta, GA, United States, 2018, https://doi.org/10.2514/6.2018-3676.

[5] Verma, S.A., Monheim, S.C., Moolchandani, K.A., Pradeep, P., Cheng, A.W., Thipphavong, D.P., Dulchinos, V.L., Arneson, H., Lauderdale, T.A., Bosson, C.S., Mueller, E.R. and Wei, B. Lessons Learned: Using UTM Paradigm for Urban Air Mobility Operations, 2020 AIAA/IEEE 39th Digital Avionics Systems Conference (DASC), 2020, https://doi.org/10.1109/DASC50938.2020.9256650.

[6] Kuchar, J.K. and Yang, L.C. A review of conflict detection and resolution modeling methods, *IEEE Trans Intell Transp Syst*, 2000, **1,** (4), pp 179–189, https://doi.org/10.1109/6979.898217.

[7] Egorov, M., Kuroda, V. and Sachs, P. Encounter aware flight planning in the unmanned airspace, 2019 Integrated Communications, Navigation and Surveillance Conference (ICNS), Herndon, VA, USA, pp 1–15, 2019, https://doi.org/10.1109/ICNSURV.2019.8735399.
[8] Wang, R., Alligier, R., Allignol, C., Barnier, N., Durand, N. and Gondran, A. Cooperation of combinatorial solvers for en-route conflict resolution, *Transp Res C: Emer Technol*, 2020, **114**, pp 36–58, https://doi.org/10.1016/j.trc.2020.01.004.
[9] Gerdes, I., Temme, A. and Schultz, M. From free-route air traffic to an adapted dynamic main-flow system, *Transp Res C: Emer Technol*, **115**, 2020, https://doi.org/10.1016/j.trc.2020.102633.
[10] Valavanis, K.P. The Entropy Based Approach to Modeling and Evaluating Autonomy and Intelligence of Robotic Systems. *J Intell Robot Syst*, 2018, **91**, pp 7–22, https://doi.org/10.1007/s10846-018-0905-6.
[11] Huang, Y., Tang, J. and Lao, S. Collision Avoidance Method for Self-Organizing Unmanned Aerial Vehicle Flights. *IEEE Access*, 2019, **7**, pp 85536–85547, https://doi.org/10.1109/ACCESS.2019.2925633.
[12] International Civil Aviation Organization. Global Air Traffic Management Operational Concept. International Civil Aviation Organization, Doc 9854, 2005.
[13] Federal Aviation Administration. Unmanned Aircraft System (UAS) Traffic Management (UTM) - Concept of Operations. U.S. Department of Transportation, Version 2.0, 2020.
[14] Rios, J. Strategic deconfliction: System requirements. National Aeronautics and Space Administration, 2018.
[15] Öreg, Zs., Shin, H. and Tsourdos, A. Traffic conflict reduction based on distributed stochastic task allocation. *Aeronaut J*, 2022, **126**, (1300), pp 993–1025, https://doi.org/10.1017/aer.2021.119.
[16] Öreg, Zs., Shin, H. and Tsourdos, A. On the underlying dynamics of traffic conflicts related to stochastic behaviour, *Proc Inst Mech Eng G*, 2022, https://doi.org/10.1177/09544100221117432.
[17] Açikmeşe, B. and Bayard, D.S. Markov Chain approach to probabilistic guidance for swarms of autonomous agents, *Asian J Cont*, 2015, **17**, (4), pp 1105–1124, https://doi.org/10.1002/asjc.982.
[18] Jang, I., Shin, H.-S. and Tsourdos, A. Local information-based control for probabilistic swarm distribution guidance. *Swarm Intell*, 2018, **12**, pp 327–359, https://doi.org/10.1007/s11721-018-0160-2.
[19] Yang, L., Han, K., Borst, C. and Mulder, M. Impact of aircraft speed heterogeneity on contingent flow control in 4D en-route operation. *Transportation Research Part C: Emerging Technologies*, 2020, **119**, https://doi.org/10.1016/j.trc.2020.102746.
[20] Kacem, T., Barreto, A., Costa, P. and Wijesekera, D. Extending ADS-B for Mixed Urban Air Traffic. 2018 IEEE/AIAA 37th Digital Avionics Systems Conference (DASC), 2018, https://doi.org/10.1109/DASC.2018.8569853.
[21] Sunil, E., Hoekstra, J., Ellerbroek, J., Bussink, F., Nieuwenhuisen, D., Vidosavljevic, A. and Kern, S. Metropolis: Relating airspace structure and capacity for extreme traffic densities, *11th USA/EUROPE Air Traffic Management R&D Seminar*, 2015.
[22] Kelly, W.E. Conflict detection and alerting for separation assurance systems, Gateway to the New Millennium. 18th Digital Avionics Systems Conference. Proceedings (Cat. No.99CH37033), Vol. 2, 1999, https://doi.org/10.1109/DASC.1999.821978.
[23] Tang, J., Zhu, F. and Piera, M.A. A causal encounter model of traffic collision avoidance system operations for safety assessment and advisory optimization in high-density airspace. *Transp Res C: Emer Technol*, 2018, **96**, pp 347–365, https://doi.org/10.1016/j.trc.2018.10.006.
[24] Mitici, M. and Blom, H.A.P. Mathematical models for air traffic conflict and collision probability estimation, *IEEE Trans Intell Transp Syst*, 2019, **20**, (3), https://doi.org/10.1109/TITS.2018.2839344.
[25] Owen, M.P., Panken, A., Moss, R., Alvarez, L. and Leeper, C. ACAS Xu: Integrated collision avoidance and detect and avoid capability for UAS, 2019 IEEE/AIAA 38th Digital Avionics Systems Conference (DASC), San Diego, CA, USA, 2019, https://doi.org/10.1109/DASC43569.2019.9081758.
[26] Alvarez, L.E., Jessen, I., Owen, M.P., Silbermann, J. and Wood, P. ACAS sXu: Robust decentralized detect and avoid for small unmanned aircraft systems, 2019 IEEE/AIAA 38th Digital Avionics Systems Conference (DASC), San Diego, CA, USA, 2019, https://doi.org/10.1109/DASC43569.2019.9081631.
[27] Li, S., Egorov, M. and Kochenderfer, M.J. Optimizing Collision Avoidance in Dense Airspace using Deep Reinforcement Learning. *Thirteenth USA/Europe Air Traffic Management Research and Development Seminar (ATM2019)*, Vienna, Austria, 2019, http://atmseminar.org/seminarContent/seminar13/papers/ATM_Seminar_2019_paper_65.pdf.
[28] Bilimoria, K.D. A geometric optimization approach to aircraft conflict resolution, AIAA Guidance, Navigation, and Control Conference and Exhibit, 2000, https://doi.org/10.2514/6.2000-4265.
[29] van den Berg, J., Guy, S.J., Lin, M. and Manocha, D. Reciprocal n-body collision avoidance, *Robot Res*, 2011, https://doi.org/10.1007/978-3-642-19457-3_1.
[30] Zhong, Z. and Xuejun, Z. An improved geometric approach to conflict resolution in curve trajectory, 9th International Conference on Electronic Measurement & Instruments, 2009, https://doi.org/10.1109/ICEMI.2009.5274889.
[31] Rebollo, J.J., Ollero, A. and Maza, I. Collision avoidance among multiple aerial robots and other non-cooperative aircraft based on velocity planning, ROBOTICA 2007 - 7th Conference on Mobile Robots and Competitions, Portugal, 2007.
[32] Wan, Y., Tang, J. and Lao, S. Research on the collision avoidance algorithm for fixed-wing UAVs based on maneuver coordination and planned trajectories prediction, *Appl Sci*, 2019, **9**, (4), https://doi.org/10.3390/app9040798.
[33] Luongo, S., Di Vito, V. and Corraro, F. An advanced 3D algorithm for automatic separation assurance systems, 2012 20th Mediterranean Conference on Control & Automation (MED), Barcelona, pp 1572–1578, 2012, https://doi.org/10.1109/MED.2012.6265863.
[34] Constans, S., Fontaine, B. and Fondacci, R. Minimizing potential conflict quantity with speed control, Proceedings of the 4th EUROCONTROL Innovative Research Workshop, 6-8 December, Bretigny-sur-Orge, 2005.

https://doi.org/10.1017/aer.2023.12 Published online by Cambridge University Press

[35] Cecen, R.K. and Cetek, C. Conflict-free en-route operations with horizontal resolution manoeuvers using a heuristic algorithm, *Aeronaut J*, 2020, pp 1–19, https://doi.org/10.1017/aer.2020.5.
[36] Mahjri, I., Dhraief, A., Belghith, A. and AlMogren, A.S. SLIDE: A straight line conflict detection and alerting algorithm for multiple unmanned aerial vehicles, *IEEE Trans Mobile Comput*, 2018, **17**, (5), pp 1190–1203, https://doi.org/10.1109/TMC.2017.2750144.
[37] Wang, C.H.J., Tan, S.K. and Low, K.H. Collision risk management for non-cooperative UAS traffic in airport-restricted airspace with alert zones based on probabilistic conflict map, *Transp Res C: Emer Technol*, 2019, **109**, pp 19–39, https://doi.org/10.1016/j.trc.2019.09.017.
[38] Lin, Y. and Saripalli, S. Collision avoidance for UAVs using reachable sets, International Conference on Unmanned Aircraft Systems, ICUAS 2015, pp 226–235, 2015, https://doi.org/10.1109/ICUAS.2015.7152295.
[39] Yang, Y., Zhang, J., Cai, K. and Prandini, M. Multi-aircraft conflict detection and resolution based on probabilistic reach sets, *IEEE Trans Cont Syst Technol*, 2017, **25**, (1), pp 309–316, https://doi.org/10.1109/TCST.2016.2542046.
[40] Ramasamy, S., Sabatini, R. and Gardi, A. A unified analytical framework for aircraft separation assurance and UAS sense-and-avoid, *J Intell Robot Syst*, 2018, **91**, pp 735–754, https://doi.org/10.1007/s10846-017-0661-z.
[41] Shi, L. and Wu, R. A probabilistic conflict detection algorithm in terminal area based on three-dimensional Brownian motion, 2012 IEEE 11th International Conference on Signal Processing, Beijing, pp 2287–2291, 2012, https://doi.org/10.1109/ICoSP.2012.6492037.
[42] Hao, S., Zhang, Y., Cheng, S., Liu, R. and Xing, Z. Probabilistic multi-aircraft conflict detection approach for trajectory-based operation. *Transport Res C*, 2018, **95**, pp 698–712, https://doi.org/10.1016/j.trc.2018.08.010.
[43] Hernández-Romero, E., Valenzuela, A., and Rivas, D. A probabilistic approach to measure aircraft conflict severity considering wind forecast uncertainty, *Aerosp Sci Technol*, 2019, **86**, pp 401–414, https://doi.org/10.1016/j.ast.2019.01.024.
[44] Hernández-Romero, E. Probabilistic aircraft conflict detection and resolution under the effects of weather uncertainty. PhD Thesis, Universidad de Sevilla, Sevilla, 2020, https://hdl.handle.net/11441/102299.
[45] Weinert, A., Campbell, S., Vela, A., Schuldt, D. and Kurucar, J. Well-clear recommendation for small unmanned aircraft systems based on unmitigated collision risk, *J Air Transport*, 2018, **26**, (3), pp 113–122, https://doi.org/10.2514/1.D0091.
[46] Lester, E.T. and Weinert, A. Three quantitative means to remain well clear for small UAS in the terminal area, 2019 Integrated Communications, Navigation and Surveillance Conference (ICNS), Herndon, VA, USA, 2019, https://doi.org/10.1109/ICNSURV.2019.8735171.
[47] ASTM F3442/F3442M-20, Standard Specification for Detect and Avoid System Performance Requirements. ASTM International, West Conshohocken, PA, 2020, https://doi.org/10.1520/F3442_F3442M-20.
[48] Hayya, J., Armstrong, D. and Gressis, N. A Note on the Ratio of Two Normally Distributed Variables. *Manag Sci*, 1975, **21**, (11), pp 1338–1341, https://doi.org/10.1287/mnsc.21.11.1338.
[49] Hinkley, D.V. On the ratio of two correlated normal random variables. *Biometrika* **56**, 3, p. 635, 1969.
[50] Cedilnik, A., Košmelj, K. and Blejec, A. The distribution of the ratio of jointly normal variables, *Metodološki zvezki*, 2004, **1**, (1), pp 99–108.
[51] Sigman, K. Lecture notes on simulation, 2010, http://www.columbia.edu/ ks20/4404-Sigman/4404-Notes-ITM.pdf.
[52] Sun, J. The 1090 Megahertz Riddle - A Guide to Decoding Mode S and ADS-B Signals. TU Delft Open Publishing, 2020, https://mode-s.org/decode/book-the_1090mhz_riddle-junzi_sun.pdf.

Appendix

A. Conflict probabilities for exponential distribution

A.1 Formulae related to exponential distribution algebra

The probability distribution of the sum $(x + y = z)$ of exponentially distributed random variables can be calculated according to Equations (A1), (A2), (A3) and (A4).

$$f_{x+y}(x, y\,; a, b) = \begin{cases} -\dfrac{ab\left(e^{-az} - e^{-bz}\right)}{a-b} \left(= \int_0^z a\,b\,e^{-ax}\,e^{-b(z-x)}\,\mathrm{d}x\right) & \text{if } z \geq 0 \text{ and } a \neq b \\ 0 & \text{if } z < 0 \text{ and } a \neq b \end{cases} \tag{A1}$$

$$f_{x+y}(x, y; a, b) = \begin{cases} a^2 z e^{-az} & \text{if } z \geq 0 \text{ and } a = b \\ 0 & \text{if } z < 0 \text{ and } a = b \end{cases} \tag{A2}$$

$$F_{x+y}(x, y; a, b) = \begin{cases} \dfrac{a\left(-e^{-bZ}\right) + b\left(e^{-aZ} - 1\right) + a}{a-b} \left(= \int_0^Z -\dfrac{ab\left(e^{-az} - e^{-bz}\right)}{a-b}\,dz\right) & \text{if } Z \geq 0 \text{ and } a \neq b \\ 0 & \text{if } Z < 0 \text{ and } a \neq b \end{cases} \tag{A3}$$

https://doi.org/10.1017/aer.2023.12 Published online by Cambridge University Press

$$F_{x+y}(x,y;a,b)=\begin{cases}1-e^{-aZ}(aZ+1) & \text{if } Z\geq 0 \text{ and } a=b\\ 0 & \text{if } Z<0 \text{ and } a=b\end{cases} \tag{A4}$$

Since the set of possible values for a truncated exponential distribution is bounded, the sum of variables with truncated exponential distributions is bounded. The probability density function and the cumulative distribution function of the sum of variables are given by Equations (A5), (A6), (A7) and (A8).

$$f'_{x+y}(x,y;a,b,l,u)=\begin{cases}\dfrac{a\,b\,e^{u(a+b)}\left(e^{2bl-bz}-e^{2al-az}\right)}{(a-b)\left(e^{al}-e^{au}\right)\left(e^{bl}-e^{bu}\right)} & \text{if } 2l\leq z\leq l+u \text{ and } a\neq b\\ \dfrac{a\,b\,e^{l(a+b)}\left(e^{2au-az}-e^{2bu-bz}\right)}{(a-b)\left(e^{al}-e^{au}\right)\left(e^{bl}-e^{bu}\right)} & \text{if } l+u<z\leq 2u \text{ and } a\neq b\\ 0 & \text{if } z<2l \text{ or } 2u<z \text{ and } a\neq b\end{cases} \tag{A5}$$

$$f'_{x+y}(x,y;a,b,l,u)=\begin{cases}-\dfrac{a^2(2l-z)e^{a(2l+2u-z)}}{\left(e^{al}-e^{au}\right)^2} & \text{if } 2l\leq z\leq l+u \text{ and } a=b\\ \dfrac{a^2(2u-z)e^{a(2l+2u-z)}}{\left(e^{al}-e^{au}\right)^2} & \text{if } l+u<z\leq 2u \text{ and } a=b\\ 0 & \text{if } z<2l \text{ or } 2u<z \text{ and } a=b\end{cases} \tag{A6}$$

$$F'_{x+y}(x,y;a,b,l,u)=\begin{cases}\dfrac{e^{u(a+b)}\left(a\left(-e^{2bl-bZ}\right)+b\left(e^{2al-aZ}-1\right)+a\right)}{(a-b)\left(e^{al}-e^{au}\right)\left(e^{bl}-e^{bu}\right)} & \text{if } 2l\leq Z\leq l+u \text{ and } a\neq b\\ \dfrac{a\left(e^{al+b(l+2u-Z)}-e^{au+bl}-e^{al+bu}+e^{u(a+b)}\right)}{(a-b)\left(e^{al}-e^{au}\right)\left(e^{bl}-e^{bu}\right)} & \\ -\dfrac{b\left(e^{a(l+2u-Z)+bl}-e^{au+bl}-e^{al+bu}+e^{u(a+b)}\right)}{(a-b)\left(e^{al}-e^{au}\right)\left(e^{bl}-e^{bu}\right)} & \text{if } l+u<Z\leq 2u \text{ and } a\neq b\\ 0 & \text{if } Z<2l \text{ and } a\neq b\\ 1 & \text{if } 2u<Z \text{ and } a\neq b\end{cases} \tag{A7}$$

$$F'_{x+y}(x,y;a,b,l,u)=\begin{cases}\dfrac{e^{2au}\left(e^{2al-aZ}(2al-aZ-1)+1\right)}{\left(e^{al}-e^{au}\right)^2} & \text{if } 2l\leq Z\leq l+u \text{ and } a=b\\ \dfrac{(a(Z-2u)+1)e^{2a(l+u)-aZ}-2e^{a(l+u)}+e^{2au}}{\left(e^{al}-e^{au}\right)^2} & \text{if } l+u<Z\leq 2u \text{ and } a=b\\ 0 & \text{if } Z<2l \text{ and } a=b\\ 1 & \text{if } 2u<Z \text{ and } a=b\end{cases} \tag{A8}$$

The difference ($z=x-y$) of the exponentially distributed variables can be calculated similarly, by evaluating the integral of the probability distribution functions (Equations (A9) and (A10)). If the distribution functions of the variables are truncated, the difference becomes bounded as given by Equations (A11) and (A12).

https://doi.org/10.1017/aer.2023.12 Published online by Cambridge University Press

$$f_{x-y}(x,y;a,b)=\begin{cases}\dfrac{abe^{-az}}{a+b} & \text{if } z\geq 0\\ \dfrac{abe^{bz}}{a+b} & \text{if } z<0\end{cases} \tag{A9}$$

$$F_{x-y}(x,y;a,b)=\begin{cases}1-\dfrac{ae^{-bZ}}{a+b} & \text{if } Z\geq 0\\ \dfrac{ae^{bZ}}{a+b} & \text{if } Z<0\end{cases} \tag{A10}$$

$$f'_{x-y}(x,y;a,b,l,u)=\begin{cases}\dfrac{abe^{-aZ}\left(e^{(a+b)(u+Z)}-e^{l(a+b)}\right)}{(a+b)\left(e^{al}-e^{au}\right)\left(e^{bl}-e^{bu}\right)} & \text{if } l-u\leq z\leq 0\\ \dfrac{abe^{-aZ}\left(e^{u(a+b)}-e^{(a+b)(l+Z)}\right)}{(a+b)\left(e^{al}-e^{au}\right)\left(e^{bl}-e^{bu}\right)} & \text{if } 0<z\leq u-l\\ 0 & \text{if } z<l-u \text{ or } u-l<z\end{cases} \tag{A11}$$

$$F'_{x-y}(x,y;a,b,l,u)=\begin{cases}\dfrac{e^{-aZ}\left(b\left(e^{l(a+b)}-e^{a(u+Z)+bl}\right)+a\left(e^{(a+b)(u+Z)}-e^{a(u+Z)+bl}\right)\right)}{(a+b)\left(e^{al}-e^{au}\right)\left(e^{bl}-e^{bu}\right)} & \text{if } l-u\leq Z\leq 0\\ 1+\dfrac{be^{-aZ}\left(e^{a(l+Z)+bu}-e^{u(a+b)}\right)}{(a+b)\left(e^{al}-e^{au}\right)\left(e^{bl}-e^{bu}\right)} & \\ +\dfrac{ae^{-aZ}\left(e^{a(l+Z)+bu}-e^{(a+b)(l+Z)}\right)}{(a+b)\left(e^{al}-e^{au}\right)\left(e^{bl}-e^{bu}\right)} & \text{if } 0<Z\leq u-l\\ 0 & \text{if } Z<l-u\\ 1 & \text{if } u-l<Z\end{cases} \tag{A12}$$

For conflict probability calculation of aircraft with perpendicular velocities it is necessary to determine the ratio ($z=x/y$) of exponentially distributed random variables. The probability density function and the cumulative distribution function for the ratio are given by Equations (A13) and (A14).

$$f_{\frac{x}{y}}(x,y;a,b)=\begin{cases}\dfrac{ab}{(az+b)^2} & \text{if } z\geq 0\\ 0 & \text{if } z<0\end{cases} \tag{A13}$$

$$F_{\frac{x}{y}}(x,y;a,b)=\begin{cases}\dfrac{aZ}{aZ+b} & \text{if } Z\geq 0\\ 0 & \text{if } Z<0\end{cases} \tag{A14}$$

If the exponential distribution variables are truncated, their ratio becomes bounded. The probability density function and the cumulative distribution function of the truncated cases are given by Equations (A15) and (A16).

https://doi.org/10.1017/aer.2023.12 Published online by Cambridge University Press

$$f'_{\frac{x}{y}}(x,y;a,b,l,u)=\begin{cases}\dfrac{abe^{au+bl}\left(z(auz+bu+1)e^{a(l-uz)}-(alz+bl+z)e^{b\left(u-\frac{l}{z}\right)}\right)}{z(az+b)^2\left(e^{au}-e^{al}\right)\left(e^{bl}-e^{bu}\right)} & \text{if } l/u\le z\le 1\\ \dfrac{abe^{\frac{(z-1)(bu-alz)}{z}}\left(z(alz+bl+1)e^{u\left(a+\frac{b}{z}\right)}-e^{l(az+b)}(auz+bu+z)\right)}{z(az+b)^2\left(e^{al}-e^{au}\right)\left(e^{bl}-e^{bu}\right)} & \text{if } 1<z\le u/l\\ 0 & \text{if } z<l/u \text{ or } u/l<z\end{cases} \tag{A15}$$

$$F'_{\frac{x}{y}}(x,y;a,b,l,u)=\begin{cases}-\dfrac{e^{au+bl}\left(b\left(e^{a(l-uz)}-1\right)+az\left(e^{b\left(u-\frac{l}{z}\right)}-1\right)\right)}{(az+b)\left(e^{au}-e^{al}\right)\left(e^{bl}-e^{bu}\right)} & \text{if } l/u\le Z\le 1\\ \dfrac{b\left(-e^{a(l(-z)+l+u)+bu}-e^{au+bl}+e^{l(a+b)}+e^{u(a+b)}\right)}{(az+b)\left(e^{al}-e^{au}\right)\left(e^{bl}-e^{bu}\right)} & \\ +\dfrac{az\left(-e^{al+b\left(l-\frac{u}{z}+u\right)}-e^{au+bl}+e^{l(a+b)}+e^{u(a+b)}\right)}{(az+b)\left(e^{al}-e^{au}\right)\left(e^{bl}-e^{bu}\right)} & \text{if } 1<Z\le u/l\\ 0 & \text{if } Z<l/u\\ 1 & \text{if } u/l<Z\end{cases} \tag{A16}$$

A.2 Geometric intrusion for truncated exponential distribution for perpendicular intrusion

Geometric conflict probabilities perpendicular intrusions, with both the ownship and the intruder speeds assuming truncated exponential distribution are given by Equations (A17)–(A19).

$$\Pr(GC')=\begin{cases}-\dfrac{e^{au+bl}\left(b\left(e^{a(l-u\cot(\beta+\delta))}-1\right)+a\cot(\beta+\delta)\left(e^{b(u-l\tan(\beta+\delta))}-1\right)\right)}{\left(e^{au}-e^{al}\right)\left(e^{bl}-e^{bu}\right)(a\cot(\beta+\delta)+b)} & \text{if } l/u\le\cot(\delta+\beta)\le 1\\ \dfrac{b\left(-e^{a(l(-\cot(\beta+\delta))+l+u)+bu}-e^{au+bl}+e^{l(a+b)}+e^{u(a+b)}\right)}{\left(e^{al}-e^{au}\right)\left(e^{bl}-e^{bu}\right)(a\cot(\beta+\delta)+b)} & \\ +\dfrac{a\cot(\beta+\delta)\left(-e^{al+b(l-u\tan(\beta+\delta)+u)}-e^{au+bl}+e^{l(a+b)}+e^{u(a+b)}\right)}{\left(e^{al}-e^{au}\right)\left(e^{bl}-e^{bu}\right)(a\cot(\beta+\delta)+b)} & \text{if } 1<\cot(\delta+\beta)\le u/l\\ 0 & \text{if } \cot(\delta+\beta)<l/u\\ 1 & \text{if } u/l\le\cot(\delta+\beta)\end{cases} \tag{A17}$$

$$\text{if } -\beta\le\delta\le\beta$$

https://doi.org/10.1017/aer.2023.12 Published online by Cambridge University Press

$$\Pr(\mathrm{GC}') = \begin{cases} -\dfrac{e^{au+bl}\left(b\left(e^{a(l+u\cot(\beta-\delta))}-1\right)-a\cot(\beta-\delta)\left(e^{b(l\tan(\beta-\delta)+u)}-1\right)\right)}{\left(e^{au}-e^{al}\right)\left(e^{bl}-e^{bu}\right)\left(b-a\cot(\beta-\delta)\right)} & \text{if } l/u \le \cot(\delta+\beta) \le 1 \\ \dfrac{b\left(-e^{a(l\cot(\beta-\delta)+l+u)+bu}-e^{au+bl}+e^{l(a+b)}+e^{u(a+b)}\right)}{\left(e^{al}-e^{au}\right)\left(e^{bl}-e^{bu}\right)\left(b-a\cot(\beta-\delta)\right)} & \\ -\dfrac{a\cot(\beta-\delta)\left(-e^{al+b(l+u\tan(\beta-\delta)+u)}-e^{au+bl}+e^{l(a+b)}+e^{u(a+b)}\right)}{\left(e^{al}-e^{au}\right)\left(e^{bl}-e^{bu}\right)\left(b-a\cot(\beta-\delta)\right)} & \text{if } 1 < \cot(\delta+\beta) \le u/l \\ 0 & \text{if } \cot(\delta+\beta) < l/u \\ 1 & \text{if } u/l \le \cot(\delta+\beta) \end{cases}$$

$$\text{if } \beta \le \delta \le \frac{\pi}{2} - \beta \tag{A18}$$

$$\Pr(\mathrm{GC}') = \begin{cases} -\dfrac{e^{au+bl}\left(b\left(e^{a(l+u\cot(\beta-\delta))}-1\right)-a\cot(\beta-\delta)\left(e^{b(l\tan(\beta-\delta)+u)}-1\right)\right)}{\left(e^{au}-e^{al}\right)\left(e^{bl}-e^{bu}\right)\left(b-a\cot(\beta-\delta)\right)} & \text{if } l/u \le \cot(\delta+\beta) \le 1 \\ \dfrac{b\left(-e^{a(l\cot(\beta-\delta)+l+u)+bu}-e^{au+bl}+e^{l(a+b)}+e^{u(a+b)}\right)}{\left(e^{al}-e^{au}\right)\left(e^{bl}-e^{bu}\right)\left(b-a\cot(\beta-\delta)\right)} & \\ -\dfrac{a\cot(\beta-\delta)\left(-e^{al+b(l+u\tan(\beta-\delta)+u)}-e^{au+bl}+e^{l(a+b)}+e^{u(a+b)}\right)}{\left(e^{al}-e^{au}\right)\left(e^{bl}-e^{bu}\right)\left(b-a\cot(\beta-\delta)\right)} & \text{if } 1 < \cot(\delta+\beta) \le u/l \\ 0 & \text{if } \cot(\delta+\beta) < l/u \\ 1 & \text{if } u/l \le \cot(\delta+\beta) \end{cases}$$

$$\text{if } \frac{\pi}{2} - \beta \le \delta \le \frac{\pi}{2} + \beta \tag{A19}$$

A.3 Geometric intrusion for exponential distribution with arbitrary intrusion angle

The conflict probabilities for $0 < \theta < \pi$ can then be calculated according to Equation (A20). If $\theta = 0$, the conflict probability is the same as given by Equation (26), if $\theta = \pi$ Equation (27) gives the conflict probability. For $-\pi < \theta < 0$ the conflict probabilities can be calculated similarly, and are given by Equation (A21). For truncated distributions the distribution of $\tan\Omega$ (Equation (30)) becomes Equation (A23). For $-\pi < \theta < 0$ a different formula is used, which is given by Equation (A25). Using Equation (A23) the conflict probabilities can be calculated according to Equation (A22).

https://doi.org/10.1017/aer.2023.12 Published online by Cambridge University Press

$$
\begin{cases}
\dfrac{b}{a\sin(\theta)\cot(\beta+\delta)-a\cos(\theta)+b} & \text{if } -\beta \le \delta \le \beta \text{ and } \cot(\beta+\delta) \ge \cot\theta \\
1 & \text{if } -\beta \le \delta \le \beta \text{ and } \cot(\beta+\delta) < \cot\theta \\
0 & \text{if } \beta < \delta < \pi-\beta \text{ and } \cot(\delta-\beta) < \cot\theta \\
\dfrac{b}{a\sin(\theta)\cot(\beta+\delta)-a\cos(\theta)+b}-1 & \text{if } \beta < \delta < \pi-\beta \text{ and } \cot(\delta-\beta) < \cot\theta \\
 & \text{and } \cot(\delta-\beta) \ge \cot\theta \\
\dfrac{a}{a-b\sin(\beta-\delta)\csc(\beta-\delta+\theta)} & \text{if } \beta < \delta < \pi-\beta \text{ and } \cot(\delta-\beta) \ge \cot\theta \\
 & \text{and } \cot(\delta-\beta) < \cot\theta \\
\dfrac{a}{a-b\sin(\beta-\delta)\csc(\beta-\delta+\theta)} & \\
+\dfrac{b}{a\sin(\theta)\cot(\beta+\delta)-a\cos(\theta)+b}-1 & \text{if } \beta < \delta < \pi-\beta \text{ and } \cot(\delta-\beta) \ge \cot\theta \\
 & \text{and } \cot(\delta-\beta) \ge \cot\theta \\
\dfrac{a}{a-b\sin(\beta-\delta)\csc(\beta-\delta+\theta)} & \text{if } (-\pi \le \delta \le -\pi+\beta \text{ or } \pi-\beta \le \delta \le \pi) \\
 & \text{and } \cot(\delta-\beta) \ge \cot\theta \\
0 & \text{if } (-\pi \le \delta \le -\pi+\beta \text{ or } \pi-\beta \le \delta \le \pi) \\
 & \text{and } \cot(\delta-\beta) < \cot\theta
\end{cases}
\tag{A20}
$$

https://doi.org/10.1017/aer.2023.12 Published online by Cambridge University Press

$$
\begin{cases}
1 & \text{if } -\beta \le \delta \le \beta \text{ and } \cot(\beta+\delta) \ge \cot\theta \\
\dfrac{b}{b - a\sin(\theta)(\cot(\beta-\delta)+\cot(\theta))} & \text{if } -\beta \le \delta \le \beta \text{ and } \cot(\beta+\delta) < \cot\theta \\
0 & \text{if } \beta < \delta < \pi - \beta \\
1 - \dfrac{b}{b - a\sin(\theta)(\cot(\beta-\delta)+\cot(\theta))} & \text{if } -\pi + \beta \le \delta < -\beta \text{ and } \cot(\delta+\beta) \ge \cot\theta \\
 & \text{and } \cot(\delta-\beta) < \cot\theta \\
\dfrac{b}{b - a\sin(\theta)(\cot(\theta)-\cot(\beta+\delta))} & \\
-\dfrac{b}{b - a\sin(\theta)(\cot(\beta-\delta)+\cot(\theta))} & \text{if } -\pi + \beta \le \delta < -\beta \text{ and } \cot(\delta+\beta) < \cot\theta \\
 & \text{and } \cot(\delta-\beta) < \cot\theta \\
0 & \text{if } -\pi + \beta \le \delta < -\beta \text{ and } \cot(\delta+\beta) \ge \cot\theta \\
 & \text{and } \cot(\delta-\beta) \ge \cot\theta \\
0 & \text{if } (-\pi \le \delta \le -\pi + \beta \text{ or } \pi - \beta \le \delta \le \pi) \\
 & \text{and } \cot(\delta-\beta) \ge \cot\theta \\
1 - \dfrac{b}{b - a\sin(\theta)(\cot(\theta)-\cot(\beta+\delta))} & \text{if } (-\pi \le \delta \le -\pi + \beta \text{ or } \pi - \beta \le \delta \le \pi) \\
 & \text{and } \cot(\delta-\beta) < \cot\theta \\
 & \text{and } \delta + \beta < \theta
\end{cases}
\tag{A21}
$$

https://doi.org/10.1017/aer.2023.12 Published online by Cambridge University Press

$$
\begin{cases}
\dfrac{a}{a+b} & \text{if } -\pi \le \delta < -\pi+\beta \text{ and } \theta = -\pi \\
\Pr'(\tan\Omega \le \cot(-\beta-\delta)) & \text{if } -\pi \le \delta < -\pi+\beta \text{ and } -\pi < \theta < 0 \\
\Pr(\tan\Omega \le \cot(\delta-\beta)) & \text{if } -\pi \le \delta < -\pi+\beta \text{ and } 0 < \theta < \pi \\
\dfrac{a}{a+b} & \text{if } -\pi \le \delta < -\pi+\beta \text{ and } \theta = \pi \\
\Pr'(\tan\Omega \le \cot(-\delta-\beta)) & \\
-\Pr'(\tan\Omega \le \cot(-\delta+\beta)) & \text{if } -\pi+\beta \le \delta < -\beta \text{ and } -\pi < \theta < 0 \\
1-\dfrac{a}{a+b} & \text{if } -\beta \le \delta < \beta \text{ and } \theta = -\pi \\
1-\Pr'(\tan\Omega \le \cot(\beta-\delta)) & \text{if } -\beta \le \delta < \beta \text{ and } \pi < \theta < 0 \\
1 & \text{if } -\beta \le \delta < \beta \text{ and } \theta = 0 \\
1-\Pr(\tan\Omega \le \cot(\beta+\delta)) & \text{if } -\beta \le \delta < \beta \text{ and } 0 < \theta < \pi \\
1-\dfrac{a}{a+b} & \text{if } -\beta \le \delta < \beta \text{ and } \theta = \pi \\
\Pr(\tan\Omega \le \cot(\delta-\beta)) & \\
-\Pr(\tan\Omega \le \cot(\beta+\delta)) & \text{if } \beta \le \delta < \pi-\beta \text{ and } 0 < \theta < \pi \\
\dfrac{a}{a+b} & \text{if } \pi-\beta \le \delta \le \pi \text{ and } \theta = -\pi \\
\Pr'(\tan\Omega \le \cot(-\beta-\delta)) & \text{if } \pi-\beta \le \delta \le \pi \text{ and } -\pi < \theta < 0 \\
\Pr(\tan\Omega \le \cot(\delta-\beta)) & \text{if } \pi-\beta \le \delta \le \pi \text{ and } 0 < \theta < \pi \\
\dfrac{a}{a+b} & \text{if } \pi-\beta \le \delta \le \pi \text{ and } \theta = \pi \\
0 & \text{else}
\end{cases}
\tag{A22}
$$

https://doi.org/10.1017/aer.2023.12 Published online by Cambridge University Press

$$\Pr(\tan\Omega \le Z)$$

$$= \begin{cases} \dfrac{-e^{au+bl}\, b\left(e^{a(l-u\sin(\theta)(\cot(\theta)+Z))}-1\right)}{\left(e^{au}-e^{al}\right)\left(e^{bl}-e^{bu}\right)\left(a\sin(\theta)(\cot(\theta)+Z)+b\right)} \\ \quad - \dfrac{ae^{au+bl}\sin(\theta)(\cot(\theta)+Z)\left(e^{b\left(u-\frac{l\csc(\theta)}{\cot(\theta)+Z}\right)}-1\right)}{\left(e^{au}-e^{al}\right)\left(e^{bl}-e^{bu}\right)\left(a\sin(\theta)(\cot(\theta)+Z)+b\right)} & \text{if } \dfrac{l}{u} < (Z+\cot\theta)\sin\theta \\ & \text{and } (Z+\cot\theta)\sin\theta \le 1 \\ \dfrac{b\left(-\exp\left(a(l\sin(\theta)(-(\cot(\theta)+Z))+l+u)+bu\right)-e^{au+bl}+e^{l(a+b)}+e^{u(a+b)}\right)}{\left(e^{al}-e^{au}\right)\left(e^{bl}-e^{bu}\right)\left(a\sin(\theta)(\cot(\theta)+Z)+b\right)} \\ \quad + \dfrac{a\sin(\theta)(\cot(\theta)+Z)\left(-e^{al+b\left(l-\frac{u\csc(\theta)}{\cot(\theta)+Z}+u\right)}-e^{au+bl}+e^{l(a+b)}+e^{u(a+b)}\right)}{\left(e^{al}-e^{au}\right)\left(e^{bl}-e^{bu}\right)\left(a\sin(\theta)(\cot(\theta)+Z)+b\right)} & \text{if } \dfrac{u}{l} > (Z+\cot\theta)\sin\theta \\ & \text{and } (Z+\cot\theta)\sin\theta > 1 \\ 0 & \text{else} \end{cases} \tag{A23}$$

$$\Pr'(\tan\Omega \le Z)$$

$$= \begin{cases} \dfrac{-e^{au+bl}\, b\left(e^{a(l+u\sin(\theta)(\cot(\theta)+Z))}-1\right)}{\left(e^{au}-e^{al}\right)\left(e^{bl}-e^{bu}\right)\left(b-a\sin(\theta)(\cot(\theta)+Z)\right)} \\ \quad + \dfrac{e^{au+bl}\, a\sin(\theta)(\cot(\theta)+Z)\left(e^{b\left(\frac{l\csc(\theta)}{\cot(\theta)+Z}+u\right)}-1\right)}{\left(e^{au}-e^{al}\right)\left(e^{bl}-e^{bu}\right)\left(b-a\sin(\theta)(\cot(\theta)+Z)\right)} & \text{if } \dfrac{l}{u} < -(Z+\cot\theta)\sin\theta \\ & \text{and } -(Z+\cot\theta)\sin\theta \le 1 \\ \dfrac{b\left(-e^{a(l\sin(\theta)(\cot(\theta)+Z)+l+u)+bu}-e^{au+bl}+e^{l(a+b)}+e^{u(a+b)}\right)}{\left(e^{al}-e^{au}\right)\left(e^{bl}-e^{bu}\right)\left(b-a\sin(\theta)(\cot(\theta)+Z)\right)} \\ \quad - \dfrac{a\sin(\theta)(\cot(\theta)+Z)\left(-e^{al+b\left(l+\frac{u\csc(\theta)}{\cot(\theta)+Z}+u\right)}-e^{au+bl}+e^{l(a+b)}+e^{u(a+b)}\right)}{\left(e^{al}-e^{au}\right)\left(e^{bl}-e^{bu}\right)\left(b-a\sin(\theta)(\cot(\theta)+Z)\right)} & \text{if } \dfrac{u}{l} > -(Z+\cot\theta)\sin\theta \\ & \text{and } -(Z+\cot\theta)\sin\theta > 1 \\ 0 & \text{else} \end{cases} \tag{A24}$$

https://doi.org/10.1017/aer.2023.12 Published online by Cambridge University Press

A.4 Speed intrusion for full exponential distribution for perpendicular intrusion

Case 1: $-\beta \le \delta \le \beta$

$$\int_{\frac{r_S-r_C}{t_{\rm th}}}^{\infty} \int_0^{x\cot\left(\frac{\pi}{2}-(\beta+\delta)\right)} a\,b\,e^{-ax}\,e^{-by}\,\mathrm{d}y\,\mathrm{d}x \le \Pr(\mathrm{SC}) =$$

$$1 - \int_0^{\frac{d(\delta,\gamma)}{t_{\rm th}}} \int_0^{\frac{\pi}{2}-(\beta+\delta)} a\,b\,v_R\,e^{-av_R\sin(\gamma)}\,e^{-bv_R\cos(\gamma)}\,\mathrm{d}\gamma\,\mathrm{d}v_R$$

$$\le \int_{\frac{(r_S-r_C)\sin\left(\frac{\pi}{2}-(\beta+\delta)\right)}{t_{\rm th}}}^{\infty} \int_0^{x\cot\left(\frac{\pi}{2}-(\beta+\delta)\right)} a\,b\,e^{-ax}\,e^{-by}\,\mathrm{d}y\,\mathrm{d}x \tag{A25}$$

Case 2: $\beta \le \delta \le \frac{\pi}{4}$

$$\int_{\frac{\sqrt{r_S^2-r_C^2}}{t_{\rm th}}}^{\infty} \int_0^{x\cot\left(\frac{\pi}{2}-(\beta+\delta)\right)} a\,b\,e^{-ax}\,e^{-by}\,\mathrm{d}y\,\mathrm{d}x - \int_{\frac{\sqrt{r_S^2-r_C^2}}{t_{\rm th}}}^{\infty} \int_0^{x\cot\left(\frac{\pi}{2}-(\delta-\beta)\right)} a\,b\,e^{-ax}\,e^{-by}\,\mathrm{d}y\,\mathrm{d}x \le$$

$$\begin{aligned}\Pr(\mathrm{SC}) = 1 &- \int_0^{\frac{d(\delta,\gamma)}{t_{\rm th}}} \int_0^{\frac{\pi}{2}-(\beta+\delta)} a\,b\,v_R\,e^{-av_R\sin(\gamma)}\,e^{-bv_R\cos(\gamma)}\,\mathrm{d}\gamma\,\mathrm{d}v_R \\ &- \int_0^{\frac{d(\delta,\gamma)}{t_{\rm th}}} \int_{\frac{\pi}{2}-(\delta-\beta)}^{\frac{\pi}{2}} a\,b\,v_R\,e^{-av_R\sin(\gamma)}\,e^{-bv_R\cos(\gamma)}\,\mathrm{d}\gamma\,\mathrm{d}v_R \\ &\le \int_{\frac{(r_S-r_C)\sin\left(\frac{\pi}{2}-(\beta+\delta)\right)}{t_{\rm th}}}^{\infty} \int_0^{x\cot\left(\frac{\pi}{2}-(\beta+\delta)\right)} a\,b\,e^{-ax}\,e^{-by}\,\mathrm{d}y\,\mathrm{d}x \\ &- \int_{\frac{(r_S-r_C)\sin\left(\frac{\pi}{2}-(\beta+\delta)\right)}{t_{\rm th}}}^{\infty} \int_0^{x\cot\left(\frac{\pi}{2}-(\delta-\beta)\right)} a\,b\,e^{-ax}\,e^{-by}\,\mathrm{d}y\,\mathrm{d}x\end{aligned} \tag{A26}$$

Case 3: $\frac{\pi}{4} \le \delta \le \frac{\pi}{2} - \beta$

$$\int_{\frac{\sqrt{r_S^2-r_C^2}}{t_{\rm th}}}^{\infty} \int_0^{y\tan\left(\frac{\pi}{2}-(\delta-\beta)\right)} a\,b\,e^{-ax}\,e^{-by}\,\mathrm{d}x\,\mathrm{d}y - \int_{\frac{\sqrt{r_S^2-r_C^2}}{t_{\rm th}}}^{\infty} \int_0^{y\tan\left(\frac{\pi}{2}-(\beta+\delta)\right)} a\,b\,e^{-ax}\,e^{-by}\,\mathrm{d}x\,\mathrm{d}y \le$$

$$\begin{aligned}\Pr(\mathrm{SC}) = 1 &- \int_0^{\frac{d(\delta,\gamma)}{t_{\rm th}}} \int_0^{\frac{\pi}{2}-(\beta+\delta)} a\,b\,v_R\,e^{-av_R\sin(\gamma)}\,e^{-bv_R\cos(\gamma)}\,\mathrm{d}\gamma\,\mathrm{d}v_R \\ &\le \int_{\frac{(r_S-r_C)\cos\left(\frac{\pi}{2}-(\delta-\beta)\right)}{t_{\rm th}}}^{\infty} \int_0^{y\tan\left(\frac{\pi}{2}-(\delta-\beta)\right)} a\,b\,e^{-ax}\,e^{-by}\,\mathrm{d}x\,\mathrm{d}y \\ &- \int_{\frac{(r_S-r_C)\cos\left(\frac{\pi}{2}-(\delta-\beta)\right)}{t_{\rm th}}}^{\infty} \int_0^{y\tan\left(\frac{\pi}{2}-(\beta+\delta)\right)} a\,b\,e^{-ax}\,e^{-by}\,\mathrm{d}x\,\mathrm{d}y\end{aligned} \tag{A27}$$

Case 4: $\frac{\pi}{2} - \beta \le \delta \le \frac{\pi}{2} + \beta$

$$\int_{\frac{r_S-r_C}{t_{\rm th}}}^{\infty} \int_0^{y\tan\left(\frac{\pi}{2}-(\delta-\beta)\right)} a\,b\,e^{-ax}\,e^{-by}\,\mathrm{d}x\,\mathrm{d}y \le$$

https://doi.org/10.1017/aer.2023.12 Published online by Cambridge University Press

$$\Pr(\mathrm{SC}) = 1 - \int_0^{\frac{d(\delta,\gamma)}{t_{\mathrm{th}}}} \int_{\frac{\pi}{2}-(\delta-\beta)}^{\frac{\pi}{2}} a\, b\, v_R\, e^{-av_R \sin(\gamma)}\, e^{-bv_R \cos(\gamma)}\, \mathrm{d}\gamma\, \mathrm{d}v_R$$

$$\leq \int_{\frac{(r_S - r_C)\cos\left(\frac{\pi}{2}-(\beta+\delta)\right)}{t_{\mathrm{th}}}}^{\infty} \int_0^{y\tan\left(\frac{\pi}{2}-(\delta-\beta)\right)} a\, b\, e^{-ax}\, e^{-by}\, \mathrm{d}x\, \mathrm{d}y \tag{A28}$$

Evaluating the integral bounds the conflict probability can be calculated (Equations (A29), (A30), (A31) and (A32)).

Case 1: $-\beta \leq \delta \leq \beta$

$$e^{-\frac{a\sqrt{r_S^2 - r_C^2}}{t_{\mathrm{th}}}} \frac{\left(a\left(-e^{-\frac{b\sqrt{r_S^2 - r_C^2}\tan(\beta+\delta)}{t_{\mathrm{th}}}}\right) + a + b\tan(\beta+\delta)\right)}{a + b\tan(\beta+\delta)} \leq \Pr(\mathrm{SC}) \leq$$

$$e^{\frac{a(r_C - r_S)\cos(\beta+\delta)}{t_{\mathrm{th}}}} \frac{\left(a\left(-e^{\frac{b(r_C - r_S)\sin(\beta+\delta)}{t_{\mathrm{th}}}}\right) + a + b\tan(\beta+\delta)\right)}{a + b\tan(\beta+\delta)} \tag{A29}$$

Case 2: $\beta \leq \delta \leq \frac{\pi}{4}$

$$ae^{-\frac{\sqrt{r_S^2 - r_C^2}(a + b\tan(\beta+\delta))}{t_{\mathrm{th}}}} \frac{\left((a + b\tan(\beta+\delta))\exp\left(\frac{2b\sin(2\beta)\sqrt{r_S^2 - r_C^2}}{t_{\mathrm{th}}(\cos(2\beta)+\cos(2\delta))}\right) - a + b\tan(\beta-\delta)\right)}{(a - b\tan(\beta-\delta))(a + b\tan(\beta+\delta))}$$

$$\leq \Pr(\mathrm{SC}) \leq$$

$$ae^{\frac{a(r_C - r_S)\cos(\beta+\delta)}{t_{\mathrm{th}}}} \left(\frac{\exp\left(\frac{b(r_C - r_S)(\sin(2\delta) - \sin(2\beta))\sec(\beta-\delta)}{2t_{\mathrm{th}}}\right)}{a - b\tan(\beta-\delta)} - \frac{e^{\frac{b(r_C - r_S)\sin(\beta+\delta)}{t_{\mathrm{th}}}}}{a + b\tan(\beta+\delta)}\right) \tag{A30}$$

Case 3: $\frac{\pi}{4} \leq \delta \leq \frac{\pi}{2} - \beta$

$$be^{-\frac{\sqrt{r_S^2 - r_C^2}(a\cot(\beta+\delta)+b)}{t_{\mathrm{th}}}} \frac{\left(-a\cot(\beta-\delta) - (a\cot(\beta+\delta)+b)\exp\left(\frac{4a\sin(\beta)\cos(\beta)\sqrt{r_S^2 - r_C^2}}{t_{\mathrm{th}}\cos(2\delta) - t_{\mathrm{th}}\cos(2\beta)}\right) + b\right)}{(b - a\cot(\beta-\delta))(a\cot(\beta+\delta)+b)}$$

$$\leq \Pr(\mathrm{SC}) \leq$$

$$be^{-\frac{(r_C - r_S)\sin(\beta-\delta)(a\cot(\beta+\delta)+b)}{t_{\mathrm{th}}}} \frac{\left(-a\cot(\beta-\delta) - (a\cot(\beta+\delta)+b)e^{\frac{a\sin(2\beta)(r_C - r_S)\csc(\beta+\delta)}{t_{\mathrm{th}}}} + b\right)}{(b - a\cot(\beta-\delta))(a\cot(\beta+\delta)+b)} \tag{A31}$$

Case 4: $\frac{\pi}{2} - \beta \leq \delta \leq \frac{\pi}{2} + \beta$

$$e^{-\frac{b\sqrt{r_S^2 - r_C^2}}{t_{\mathrm{th}}}} \frac{\left(-a\cot(\beta-\delta) + b\left(-e^{\frac{a\sqrt{r_S^2 - r_C^2}\cot(\beta-\delta)}{t_{\mathrm{th}}}}\right) + b\right)}{b - a\cot(\beta-\delta)} \leq \Pr(\mathrm{SC}) \leq$$

$$e^{\frac{b(r_C - r_S)\sin(\beta+\delta)}{t_{\mathrm{th}}}} \frac{\left(-a\cot(\beta-\delta) + b\left(-\exp\left(-\frac{a(r_C - r_S)(\sin(2\beta)+\sin(2\delta))\csc(\beta-\delta)}{2t_{\mathrm{th}}}\right)\right) + b\right)}{b - a\cot(\beta-\delta)} \tag{A32}$$

https://doi.org/10.1017/aer.2023.12 Published online by Cambridge University Press

A.5 Speed intrusion for truncated exponential distribution for perpendicular intrusion

For truncated distributions the formula conflict probability changes similarly to the transformation between Equations (A29) and (A33).

$$\begin{cases} \dfrac{e^{al+bu}\left(e^{a(u-l\cot(\beta+\delta))}-1\right)}{\left(e^{al}-e^{au}\right)\left(e^{bl}-e^{bu}\right)} - \dfrac{ae^{(a+b)(l+u)}\left(e^{-l(a\cot(\beta+\delta)+b)}-e^{-u(a+b\tan(\beta+\delta))}\right)}{\left(e^{al}-e^{au}\right)\left(e^{bl}-e^{bu}\right)(a+b\tan(\beta+\delta))} & \text{if } \dfrac{\sqrt{r_S^2-r_C^2}}{t_{\text{th}}} < l\cot(\delta+\beta) \\ & \text{and } u > l\cot(\delta+\beta) \\ \dfrac{e^{al+bu}\left(e^{a\left(u-\frac{\sqrt{r_S^2-r_C^2}}{t_{\text{th}}}\right)}-1\right)}{\left(e^{al}-e^{au}\right)\left(e^{bl}-e^{bu}\right)} - \dfrac{ae^{(a+b)(l+u)}\left(e^{-\frac{\sqrt{r_S^2-r_C^2}}{t_{\text{th}}}(a+b\tan(\beta+\delta))}-e^{-u(a+b\tan(\beta+\delta))}\right)}{\left(e^{al}-e^{au}\right)\left(e^{bl}-e^{bu}\right)(a+b\tan(\beta+\delta))} & \text{if } \dfrac{\sqrt{r_S^2-r_C^2}}{t_{\text{th}}} \geq l\cot(\delta+\beta) \\ & \text{and } u > \dfrac{\sqrt{r_S^2-r_C^2}}{t_{\text{th}}} \\ 0 & \text{else} \end{cases}$$

$$\leq \Pr(SC') \leq$$

$$\begin{cases} \dfrac{e^{al+bu}\left(e^{a(u-l\cot(\beta+\delta))}-1\right)}{\left(e^{al}-e^{au}\right)\left(e^{bl}-e^{bu}\right)} - \dfrac{ae^{(a+b)(l+u)}\left(e^{-l(a\cot(\beta+\delta)+b)}-e^{-u(a+b\tan(\beta+\delta))}\right)}{\left(e^{al}-e^{au}\right)\left(e^{bl}-e^{bu}\right)(a+b\tan(\beta+\delta))} & \text{if } \dfrac{(r_S-r_C)\cos(\beta+\delta)}{t_{\text{th}}} < l\cot(\delta+\beta) \\ & \text{and } u > l\cot(\delta+\beta) \\ \dfrac{e^{al+bu}\left(e^{a\left(\frac{(r_C-r_S)\cos(\beta+\delta)}{t_{\text{th}}}+u\right)}-1\right)}{\left(e^{al}-e^{au}\right)\left(e^{bl}-e^{bu}\right)} - \dfrac{ae^{(a+b)(l+u)}\left(e^{\frac{(r_C-r_S)\cos(\beta+\delta)(a+b\tan(\beta+\delta))}{t_{\text{th}}}}-e^{-u(a+b\tan(\beta+\delta))}\right)}{\left(e^{al}-e^{au}\right)\left(e^{bl}-e^{bu}\right)(a+b\tan(\beta+\delta))} & \text{if } \dfrac{(r_S-r_C)\cos(\beta+\delta)}{t_{\text{th}}} \geq l\cot(\delta+\beta) \\ & \text{and } u > \dfrac{(r_S-r_C)\cos(\beta+\delta)}{t_{\text{th}}} \\ 0 & \text{else} \end{cases} \tag{A33}$$

A.6 Speed intrusion for truncated exponential distribution for intrusion with arbitrary direction

Speed conflict probability is upper bounded by the case of direct opposite movement. The upper approximation of a speed conflict can be calculated similarly to Equation (A34). The lower approximation is is formulated analogously to Equation (A35).

https://doi.org/10.1017/aer.2023.12 Published online by Cambridge University Press

$$
\Pr(\mathrm{SC}) =
\begin{cases}
\min\left(\begin{cases} 1-e^{-\frac{a(r_S-r_C)}{t_{\mathrm{th}}}}\left(\dfrac{a(r_S-r_C)}{t_{\mathrm{th}}}+1\right) & a=b \\ \dfrac{a\left(-e^{-\frac{b(r_S-r_C)}{t_{\mathrm{th}}}}\right)+b\left(e^{-\frac{a(r_S-r_C)}{t_{\mathrm{th}}}}-1\right)+a}{a-b} & a\neq b \end{cases}, \right. \\
\left. \dfrac{e^{-\frac{a\csc(\theta)(r_C-r_S)\sin(\beta+\delta-\theta)}{t_{\mathrm{th}}}}\left(a\sin(\beta+\delta-\theta)\left(e^{\frac{b\csc(\theta)(r_C-r_S)\sin(\beta+\delta)}{t_{\mathrm{th}}}}-1\right)+b\sin(\beta+\delta)\right)}{b\sin(\beta+\delta)-a\sin(\beta+\delta-\theta)} \right) & \text{if } -\beta<\delta<\theta-\beta \\
1-\begin{cases} 1-e^{-\frac{a(r_S-r_C)}{t_{\mathrm{th}}}}\left(\dfrac{a(r_S-r_C)}{t_{\mathrm{th}}}+1\right) & a=b \\ \dfrac{a\left(-e^{-\frac{b(r_S-r_C)}{t_{\mathrm{th}}}}\right)+b\left(e^{-\frac{a(r_S-r_C)}{t_{\mathrm{th}}}}-1\right)+a}{a-b} & a\neq b \end{cases} & \text{if } \theta-\beta\leq\delta\leq\beta \\
\min\left(\begin{cases} 1-e^{-\frac{a(r_S-r_C)}{t_{\mathrm{th}}}}\left(\dfrac{a(r_S-r_C)}{t_{\mathrm{th}}}+1\right) & a=b \\ \dfrac{a\left(-e^{-\frac{b(r_S-r_C)}{t_{\mathrm{th}}}}\right)+b\left(e^{-\frac{a(r_S-r_C)}{t_{\mathrm{th}}}}-1\right)+a}{a-b} & a\neq b \end{cases}, \right. \\
\left. \dfrac{e^{-\frac{b\csc(\theta)(r_C-r_S)\sin(\beta-\delta)}{t_{\mathrm{th}}}}\left(a\sin(\beta-\delta+\theta)+b\sin(\beta-\delta)\left(e^{\frac{a\csc(\theta)(r_C-r_S)\sin(\beta-\delta+\theta)}{t_{\mathrm{th}}}}-1\right)\right)}{a\sin(\beta-\delta+\theta)-b\sin(\beta-\delta)} \right) & \text{if } \beta<\delta<\beta+\theta \\
0 & \text{else}
\end{cases}
\tag{A34}
$$

https://doi.org/10.1017/aer.2023.12 Published online by Cambridge University Press

$$\Pr(\mathrm{SC}) = \begin{cases} e^{-\frac{a\sqrt{r_S^2-r_C^2}}{t_{\mathrm{th}}}} & \\ \dfrac{\left(a\left(-e^{\frac{b\sqrt{r_S^2-r_C^2}\sin(\beta+\delta)\csc(\beta+\delta-\theta)}{t_{\mathrm{th}}}}\right)+a-b\sin(\beta+\delta)\csc(\beta+\delta-\theta)\right)}{a-b\sin(\beta+\delta)\csc(\beta+\delta-\theta)} & \text{if } -\beta<\delta<\theta-\beta \\ 1-\begin{cases} 1-e^{-\frac{a\sqrt{r_S^2-r_C^2}}{t_{\mathrm{th}}}}\left(\frac{a\sqrt{r_S^2-r_C^2}}{t_{\mathrm{th}}}+1\right) & a=b \\ \dfrac{a\left(-e^{-\frac{b\sqrt{r_S^2-r_C^2}}{t_{\mathrm{th}}}}\right)+b\left(e^{-\frac{a\sqrt{r_S^2-r_C^2}}{t_{\mathrm{th}}}}-1\right)+a}{a-b} & a\neq b \end{cases} & \text{if } \theta-\beta\le\delta\le\beta \\ e^{-\frac{b\sqrt{r_S^2-r_C^2}}{t_{\mathrm{th}}}} & \\ \dfrac{\left(-a\csc(\beta-\delta)\sin(\beta-\delta+\theta)+b\left(-e^{\frac{a\sqrt{r_S^2-r_C^2}\csc(\beta-\delta)\sin(\beta-\delta+\theta)}{t_{\mathrm{th}}}}\right)+b\right)}{b-a\csc(\beta-\delta)\sin(\beta-\delta+\theta)} & \text{if } \beta<\delta<\beta+\theta \\ 0 & \text{else} \end{cases} \tag{A35}$$

B. Conflict probabilities for normal distribution

B.1 Transformation of the normal distribution

The joint probability distribution for orthogonal variables is given by Equation (B1).

$$P_{x,y} = \frac{1}{2\pi\sigma_x\sigma_y} e^{-\frac{1}{2}\left(\frac{(x-\mu)^2}{\sigma_x^2}+\frac{(y-\nu)^2}{\sigma_y^2}\right)} \tag{B1}$$

Substituting $p=\sqrt{x^2+y^2}$ and $q=\frac{x}{y}$ and completing the square leads to the formula given by Equation (B2).

$$P_{p,q} = \frac{1}{\sqrt{2\pi}\sigma_p} e^{-\frac{1}{2}\left(\frac{p-\xi}{\sigma_p}\right)^2} \frac{\sigma_p}{\sqrt{2\pi}\sigma_x\sigma_y} e^{-\frac{1}{2}\kappa} \tag{B2}$$

In Equation (B2) the parameters are defined by Equation (B5).

$$\xi = \frac{\sqrt{q^2+1}\left(\nu\sigma_x^2+\mu\sigma_y^2 q\right)}{\sigma_x^2+\sigma_y^2 q^2} \tag{B3}$$

$$\sigma_p = \sqrt{\frac{\sigma_x^2\sigma_y^2\left(q^2+1\right)}{\sigma_x^2+\sigma_y^2 q^2}} \tag{B4}$$

$$\kappa = \frac{\left(\sigma_x^2+\sigma_y^2 q^2\right)\left(\frac{\mu^2\sigma_y^2+\nu^2\sigma_x^2}{\sigma_x^2+\sigma_y^2 q^2}-\frac{\left(\nu\sigma_x^2+\mu\sigma_y^2 q\right)^2}{\left(\sigma_x^2+\sigma_y^2 q^2\right)^2}\right)}{\sigma_x^2\sigma_y^2} \tag{B5}$$

Cite this article: Öreg Zs., Shin H.-S. and Tsourdos A. (2023). Analysis of the traffic conflict situation for speed probability distributions. *The Aeronautical Journal*, **127**, 1380–1434. https://doi.org/10.1017/aer.2023.12

https://doi.org/10.1017/aer.2023.12 Published online by Cambridge University Press

https://dspace.org/

Analysis of the traffic conflict situation for speed probability distributions

Öreg, Zs.; Shin, Hyo-Sang; Tsourdos, Antonios

2023-08-01
Cambridge University Press
https://doi.org/10.1017/aer.2023.12
Oreg Zs, Shin H-S, Tsourdos A. (2023) Analysis of the traffic conflict situation for speed probability distributions. The Aeronautical Journal, Volume 127, Issue 1314, August 2023, pp. 1380-1434

Downloaded from a DSpace repository. https://dspace.org/